RSC Advances

PAPER

View Article Online
View Journal | View Issue

Cite this: *RSC Adv.*, 2024, **14**, 28608

Design and evaluation of sulfadiazine derivatives as potent dual inhibitors of EGFR^{WT} and EGFR^{T790M}: integrating biological, molecular docking, and ADMET analysis†

Hany M. Abd El-Lateef,‡*[ab] Hend A. A. Ezelarab, ‡*[c] Ali M. Ali,[b] Azhaar T. Alsaggaf,[d] Wael A. Mahdi,[e] Sultan Alshehri, [e] Mohamed A. El Hamd *[fg] and Moustafa O. Aboelez *[h]

A series of derivatives (**5–14**) were synthesized through the diazotization of sulfadiazine with active methylene compounds. The chemical structures of these newly designed compounds were validated through spectral and elemental analysis techniques. The antiproliferative potential of derivatives **5–14** was assessed against three distinct cancer cell lines (A431, A549, and H1975) using the MTT assay. The results revealed that compounds **8**, **12**, and **14** exhibited the most potent antiproliferative activity, with IC_{50} values ranging from 2.31 to 7.56 μM. Notably, these values were significantly lower than those of known EGFR inhibitors, including **erlotinib**, **gefitinib**, and **osimertinib**, suggesting the potential of these derivatives as novel antiproliferative agents. Furthermore, compound **12** was identified as the most potent inhibitor of both EGFR^{WT} and EGFR^{T790M} protein kinases, with IC_{50} values of 14.5 and 35.4 nM, respectively. These results outperformed those of **gefitinib** and **osimertinib**, which exhibited IC_{50} values of 18.2 and 368.2 nM, and 57.8 and 8.5 nM, respectively. Molecular docking studies of compounds **8**, **12**, and **14** within the ATP-binding sites of both EGFR^{WT} and EGFR^{T790M} corroborated the *in vitro* results when compared to **erlotinib**, **gefitinib**, and **osimertinib**. The docking results indicated that compound **8** exhibited a favorable binding affinity for both EGFR^{WT} and EGFR^{T790M}, with binding scores of −6.40 kcal mol^{-1} and −7.53 kcal mol^{-1}, respectively, which were comparable to those of **gefitinib** and **osimertinib**, with binding scores of −8.01 and −8.72 kcal mol^{-1}, respectively. Furthermore, an assessment of the most promising EGFR inhibitors (**8**, **12**, and **14**) using the egg-boiled method for their *in silico* ADME properties revealed significant lipophilicity, blood–brain barrier (BBB) penetration, and gastrointestinal (GIT) absorption. Collectively, our designed analogs, particularly compounds **8**, **12**, and **14**, exhibit promising dual antiproliferative and EGFR^{WT} and EGFR^{T790M} kinase inhibitory properties, positioning them as efficient candidates for further therapeutic development.

Received 6th June 2024
Accepted 2nd September 2024

DOI: 10.1039/d4ra04165h

rsc.li/rsc-advances

1. Introduction

Molecular hybridization is a pivotal strategy in drug design,[1–5] involving the deliberate fusion of two or more biologically relevant pharmacophores, often bridged by a spacer or linker, to yield a novel hybrid entity with significantly enhanced activity and efficacy compared to the parent molecule.[6–9] This strategy can also decrease undesirable side effects, thereby improving the overall therapeutic index.[10–13] Moreover, recent investigations have revealed that sulfonamides possess potent growth inhibitory activity against a diverse range of tumor lines and tyrosine kinase (TK) enzymes, underscoring their potential as promising anticancer agents.

The utilization of pyrimidines as a scaffold for producing new EGFR inhibitors that target multiple pathways, particularly oncogenesis, has been correlated with the significant anticancer

[a]*Department of Chemistry, College of Science, King Faisal University, Al-Ahsa 31982, Saudi Arabia. E-mail: hmahmed@kfu.edu.sa*
[b]*Department of Chemistry, Faculty of Science, Sohag 82524, Egypt*
[c]*Department of Medicinal Chemistry, Faculty of Pharmacy, Minia University, 61519-Minia, Egypt. E-mail: hend_aly@minia.edu.eg*
[d]*Department of Chemistry, Taibah University, Madinah, Saudi Arabia*
[e]*Department of Pharmaceutics, College of Pharmacy, King Saud University, Riyadh 11451, Saudi Arabia*
[f]*Department of Pharmaceutical Chemistry, College of Pharmacy, Shaqra University, Shaqra 11961, Saudi Arabia. E-mail: aboelhamdmohamed@su.edu.sa*
[g]*Department of Pharmaceutical Analytical Chemistry, Faculty of Pharmacy, South Valley University, Qena 83523, Egypt*
[h]*Department of Pharmaceutical Chemistry, Faculty of Pharmacy, Sohag University, Sohag, Egypt. E-mail: drmoustafaaboelez@yahoo.com*

† Electronic supplementary information (ESI) available: IR spectra, ^{1}H NMR spectra, and ^{13}CNMR spectra. See DOI: https://doi.org/10.1039/d4ra04165h

‡ Equal contributed.

properties of sulfonamides. These compounds have been shown to exhibit effective activity across a multitude of pathways, including the inhibition of carbonic anhydrase, matrix metalloproteinase, NADPH reductase, histone deacetylase, and PI3K. Notably, compounds **I–III** demonstrated more pronounced activities against both HER2 and EGFR compared to **erlotinib**, with concomitant increases in Bcl-2, Bax, and caspase-3 expression levels and the induction of cell cycle arrest in the G2/M phase[12–16] (Fig. 1).

EGFR, a receptor TK, plays a significant role in maintaining epithelial tissue homeostasis and is essential for generating and regulating cellular processes. However, the overexpression of the EGFR family members can lead to aberrant cell signaling, contributing to the progression and development of certain solid tumors, including non-small cell lung cancer (NSCLC) and breast cancers.[17,18] The EGFR-TK domain comprises five distinct sites, including the ATP-binding pocket, which is comprised of (1) the adenine binding pocket, where H-bonds are formed with the adenine ring through residue amino acids; (2) the hydrophilic pocket (ribose region); (3) the hydrophobic region I, which is critical for receptor inhibition activity, although it is not targeted by ATP; (4) the hydrophobic region II, which is also essential and frequently targeted by EGFR-TKIs (tyrosine kinase inhibitors) with a Y-shaped structure; and (5) the phosphate-binding region, which influences the pharmacokinetic features of inhibitors. Importantly, most EGFR-TKIs exhibit a Y-shaped structure and possess four critical pharmacophoric properties, which are essential for their inhibitory activity.[19–22]

The first generation of EGFR-TKIs, comprising **gefitinib** and **erlotinib**, significantly enhanced the therapy landscape for NSCLC, however they were also associated with adverse effects, such as corneal damage, trichomegaly, and occasionally fatal interstitial lung disease (ILD). Furthermore, the development of acquired resistance due to EGFR-TK mutations compromised the antitumor efficacy of these treatments.[22–25] This type of mutation diminishes the selectivity of ATP-competitive agents for the kinase while increasing EGFR's sensitivity to ATP, thereby facilitating the rapid emergence of drug-resistant mechanisms.[26] Particularly, the T790M "gatekeeper" mutation in EGFR is a prevalent mechanism of resistance, frequently observed in patients who have developed resistance to 1st generation EGFR-TKIs.[27–29]

The development of second-generation EGFR-TKIs, including pelitinib and neratinib, was driven by the need to address resistance in NSCLC treatment regimens resulting from EGFR-TK mutations.[30–33] These inhibitors interact with Cys797 near the EGFR's ATP-binding groove *via* electrophilic Michael-acceptor moieties, thereby inactivating the protein. However, their non-selective inhibition of both $EGFR^{WT}$ and $EGFR^{T790M}$ led to a relatively lower maximum tolerated dose (MTD) and adverse clinical outcomes.[34–36]

Third generation EGFR-TKIs, including olmutinib[37,38] and **osimertinib** (AZD9291),[39] are characterized as irreversible covalent inhibitors with enhanced binding affinity for $EGFR^{T790M}$ and lower affinity for $EGFR^{WT}$. These inhibitors exhibit sustained sub-nanomolar IC_{50} values for prevalent activating mutations (del19 and L858R). Due to its favorable biological properties, the FDA approved AZD9291 in 2015 for patients with NSCLC therapeutic regimens with mutant EGFR. However, a 2016 safety study reported two cases of Stevens-Johnson syndrome and severe epidermal necrolysis.[40–42] AZD9291 is currently the primary 3rd generation authorized as a first-line therapy for patients with EGFR-positive activating mutations (del19 and L858R), NSCLC, and metastatic $EGFR^{T790M}$-positive NSCLC, as identified by an approved FDA test.

Investigations into the mechanisms underlying resistance to 3rd generation have revealed the presence of both primary and acquired resistant mechanisms.[40] In order to inform subsequent treatment strategies, patients experiencing NSCLC progression after 3rd generation therapies should undergo comprehensive next-generation sequencing (NGS) analysis of plasma or tissue samples to elucidate the specific resistance mechanisms employed.[35] Further research into the mechanisms of resistance to 3rd generation is imperative for the development of effective therapeutic strategies. This study examines the findings on 3rd generation resistance in aggressive NSCLC, providing a detailed examination of the underlying molecular mechanisms and discussing novel treatment approaches for addressing this complex issue. Mobocertinib (Fig. 2), the latest addition to the 3rd generation family, has been granted accelerated approval by the FDA in 2021 for the treatment of locally advanced or metastatic NSCLC harboring exon 20 insertions, thereby offering a promising therapeutic option for patients with this specific molecular subtype.

Our study aimed to design novel EGFR-TKI derivatives, incorporating the four primary pharmacophoric properties of EGFR-TKIs, with the goal of enhancing their efficacy and

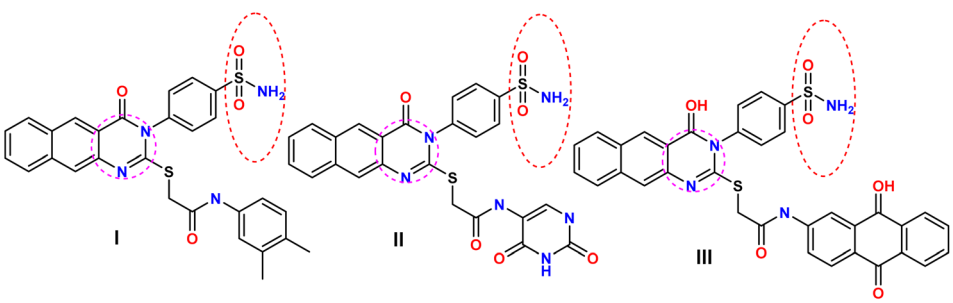

Fig. 1 Examples of sulfonamide-based derivatives as EGFR inhibitors.

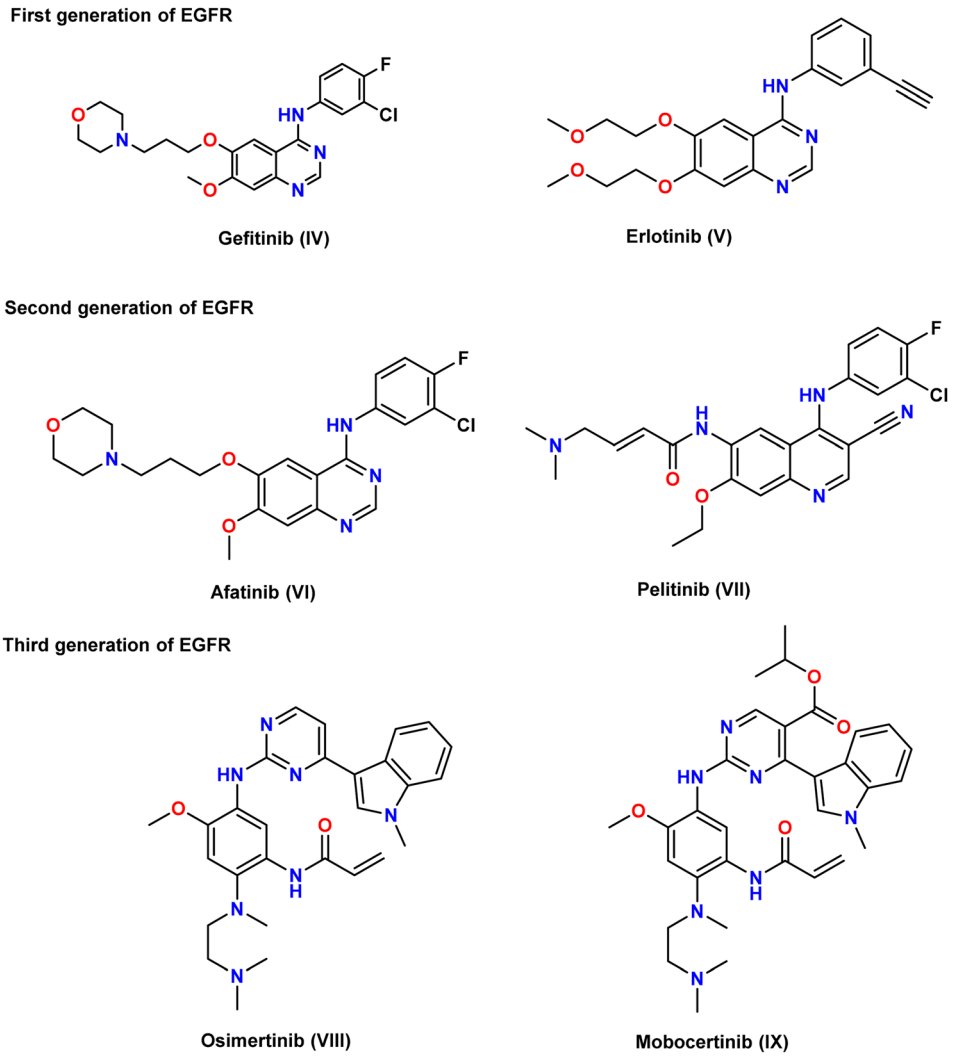

Fig. 2 The chemical structures of reported EGFR-TKIs.

selectivity. To achieve this, we synthesized a series of derivatives by structurally modifying **erlotinib** at four distinct positions (Fig. 3). Building upon our previous research focused on the scope of azole and pyrimidine derivative-based scaffolds, which have demonstrated promising antiproliferative activity against both $EGFR^{WT}$ and $EGFR^{T790M}$, we intended to further investigate the potential of these scaffolds in the development of next-generation EGFR-TKIs.

2. Results and dissection

2.1. Chemistry

In the present study, we initiated the synthesis by reacting 4-acetamidobenzene sulfonyl chloride (**1**) with 2-aminopyrimidine (**2**), resulting in the formation of *N*-(4-(*N*-(pyrimidin-2-yl)sulfamoyl)phenyl)acetamid (**3**). Subsequently, compound (**3**) was subjected to hydrolysis, yielding sulfadiazine (**4**). The next step involved the diazotization of sulfadiazine, which was then coupled with a diverse array of compounds, including ethyl acetoacetate, acetylacetone, ethyl benzoylacetate, benzoyl acetone, ethyl cyanoacetate, cyanothioacetamide, a dimer of malononitrile, diethyl malonate, *N*-[4-amino-5-cyano-6-(methylthio)pyridin-2-yl]-3-oxobutanamide, and 4,6-diamino-2-(methylthio)nicotinonitrile, in the presence of pyridine as a solvent. This reaction sequence led to the successful synthesis of hydrazone derivatives **5–14**, as illustrated in Scheme 1.

The chemical identities of the synthesized derivatives **5–14** were unequivocally confirmed through a combination of various spectral analyses. The IR spectra revealed the presence of NH_2 and NH groups, which were identified by absorption bands in the range of 3457–3103 cm^{-1}. Additionally, the IR spectra showed characteristic absorption bands for CN groups between 2215–2211 cm^{-1} and C=O groups between 1725–1655 cm^{-1}. The ^1H NMR spectra of **5–14** displayed distinct signals for NH groups, which resonated between δ 13.65–11.34 ppm. Furthermore, the ^1H NMR spectra of derivatives **5**, **7**, **9**, and **12** exhibited quartet and triplet signals for ester groups, which appeared between δ 4.37–4.23 and δ 1.29–1.24 ppm, respectively. Especially, the SCH_3 group in compound **14** was identified as a singlet at δ 2.52 ppm. The ^{13}C NMR spectra provided additional confirmation of the structures of all compounds. For example, the ^{13}C NMR spectrum of **13** showed

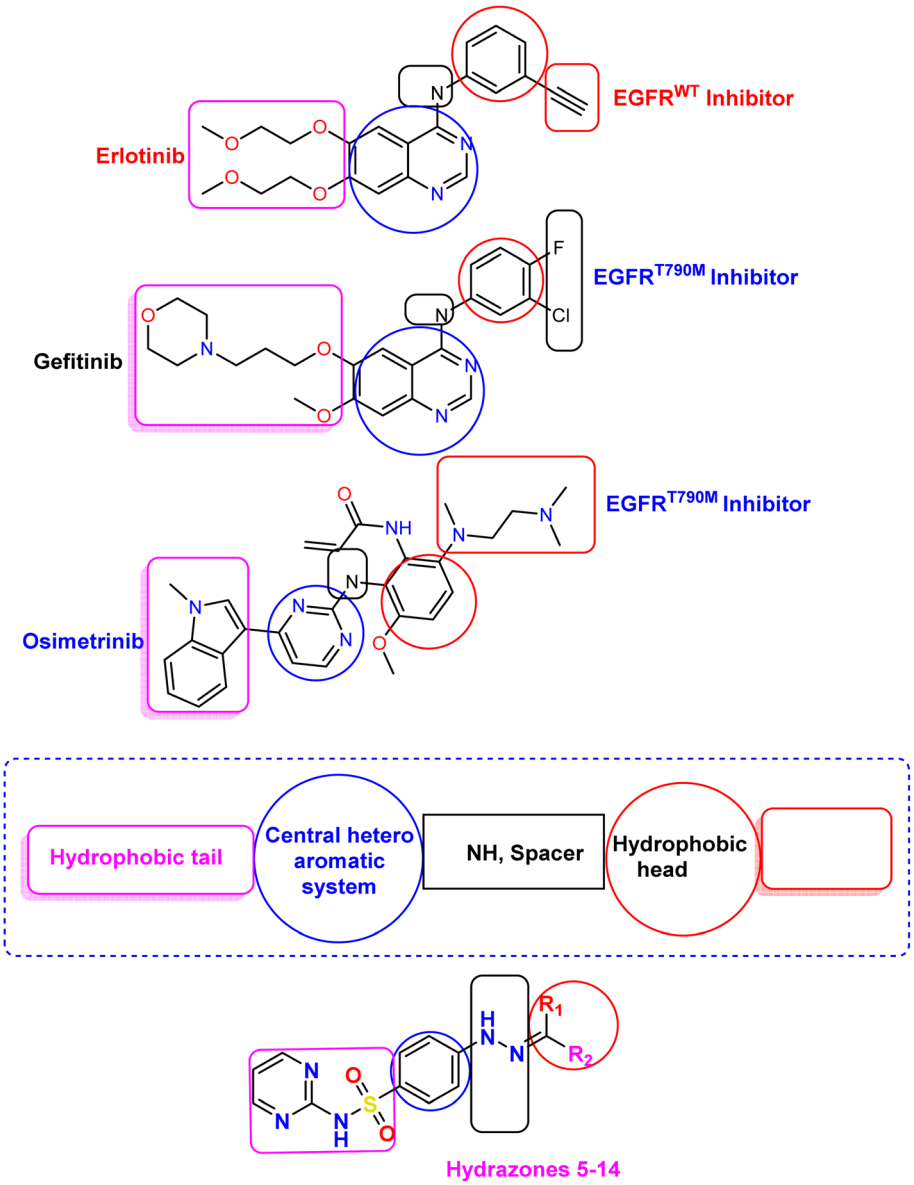

Fig. 3 Rationale design of the target derivatives utilizing **gefitinib**, **osimertinib**, and **erlotinib**.

a signal at δ 12.87 ppm, which was attributed to the SCH_3 group, and a signal at δ 79.92 ppm, which was assigned to the C–CN group. Similarly, the ^{13}C NMR spectrum of **12** revealed two distinct signals for C=O groups at δ 195.22 and 196.65 ppm, as well as a signal for a CH_3 group at δ 25.39 ppm. The elemental analysis data further verified the proposed structures of the sulfadiazine derivatives, providing a comprehensive confirmation of their chemical identities.

2.2. Biological evaluation

2.2.1. *In vitro* anti-proliferative activities. The anti-proliferative activity of the synthesized derivatives was assessed toward NSCLC cells (A549 and H1975) and human epidermoid carcinoma cells (A431) using the MTT assay method.[37–39,43–45] Notably, A431 and A549 cells overexpress $EGFR^{WT}$, whereas H1975 cells harbor the $EGFR^{T790M}$ mutation.[45] The results, presented in Table 1, reveal the IC_{50} values (μM) of the investigated derivatives, with **erlotinib**, **gefitinib**, and **osimertinib** serving as reference standards. The data indicate that compounds **8**, **12**, and **14** exhibited the most potent anti-proliferative activity, surpassing that of **gefitinib** and **erlotinib** (IC_{50} = 15.75 and 17.50 μM, respectively), with IC_{50} values ranging from 4.78 to 11.09 μM. In contrast, the remaining derivatives displayed comparable or reduced activity relative to **gefitinib** and **erlotinib**. Specifically, compounds **8**, **12**, and **14** demonstrated significant anti-proliferative activity against A431 cells, with IC_{50} values ranging from 4.78 to 7.56 μM, which exceeded the potency of **gefitinib** (IC_{50} = 9.60 μM). Particularly, compound **8** exhibited more potent anti-proliferative activity than **osimertinib**; however, its effect on the H1975 cell line was less pronounced than that of **osimertinib** (IC_{50} = 0.93 μM).

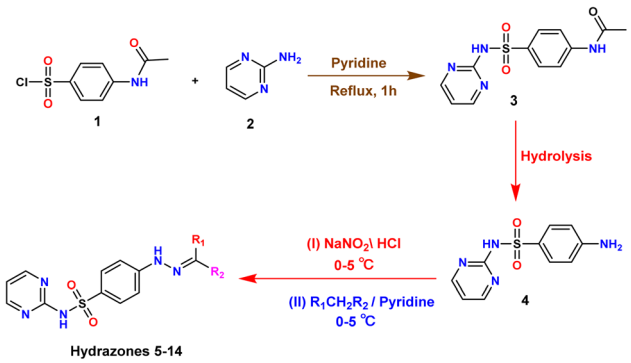

Comp.	R_1	R_2
5		
6		
7		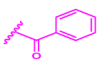
8	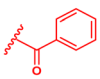	
9		
10		
11	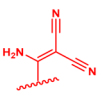	
12		
13	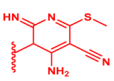	-
14		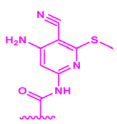

Scheme 1 Synthesis of sulfadiazine-based derivatives **5–14**.

2.2.2. EGFR^{WT} and EGFR^{T790M} kinase inhibitory activities. The sulfadiazine derivatives **5–14** were examined for their ability to inhibit the EGFR^{WT} and EGFR^{T790M} kinase enzymes employing the homogeneous time-resolved fluorescence (HTRF) KinEASE-TK assay,[40–42,46–50] with **osimertinib** and **gefitinib** as references (Table 2). The outcomes showed that the majority of the derivatives exhibited moderate inhibitory effects against EGFR^{WT}, with IC_{50} values ranging from 14.5 to 52.6 nM. Particularly, sulfadiazines **12** and **14** demonstrated significantly greater inhibitory activity against EGFR^{WT} compared to **gefitinib**. In contrast, all of the sulfadiazine derivatives **5–14** displayed improved inhibitory effects against the mutant EGFR (EGFR^{T790M}) compared to **gefitinib**. Derivative **8**, in particular, exhibited exceptional inhibitory activity, with an IC_{50} value of 9.6 nM, which was 38-fold more potent than **gefitinib**. Furthermore, derivative **8** demonstrated a comparable inhibitory effect against EGFR^{T790M} to **osimertinib**, which may account for its substantial antiproliferative effect on the H1975 cell line.

Table 1 Anti-proliferative activity of the final compounds *versus* A549, A431, and H1975

	IC_{50} (μM)[a]		
Comp.	A549	A431	H1975
5	19.24 ± 3.09	18.21 ± 0.46	20.12 ± 2.21
6	16.60 ± 0.92	17.21 ± 0.52	15.70 ± 0.21
7	11.25 ± 1.09	13.89 ± 0.80	10.32 ± 1.80
8	4.78 ± 0.12	4.12 ± 0.54	2.31 ± 0.23
9	14.98 ± 1.27	14.70 ± 0.18	13.14 ± 0.67
10	19.67 ± 0.34	18.23 ± 2.09	15.80 ± 2.48
11	13.56 ± 1.32	15.09 ± 0.58	14.13 ± 1.23
12	5.15 ± 0.30	6.38 ± 0.12	6.12 ± 0.24
13	15.45 ± 1.34	20.31 ± 2.12	17.09 ± 1.62
14	7.56 ± 0.27	6.15 ± 0.23	4.59 ± 0.43
Erlotinib	17.50 ± 2.34	11.09 ± 0.67	12.86 ± 1.23
Gefitinib	15.75 ± 1.09	9.60 ± 0.43	10.15 ± 0.39
Osimertinib	—	5.96 ± 0.63	0.93 ± 0.09

[a] IC_{50} = Mean ± SD, $n = 3$.

3. *In silico* studies

3.1. Molecular docking study

In silico simulation tests were conducted on derivatives **8**, **12**, and **14** at the active ATP binding sites of both EGFR^{WT} and EGFR^{T790M} protein kinases (PDB: 4HJO and PDB: 3W2O, respectively). The protein models were obtained from the PDB website using the MOE 2019.01 program. The results showed that the newly designed compounds docked against the EGFR^{WT} kinase with good binding affinity scores, ranging from −6.40 to −7.10 kcal mol^{-1} (Table 3). The outcomes of this

Table 2 *In vitro* enzymatic inhibitory impacts of scaffolds **5–14** *versus* EGFR^{WT} and EGFR^{T790M}

	IC_{50} (nM)	
Comp.	EGFR^{WT}	EGFR^{T790M}
5	49.2 ± 6.7	93.6 ± 8.5
6	52.6 ± 9.3	66.8 ± 10.4
7	38.9 ± 8.3	114.6 ± 9.6
8	23.2 ± 0.1	9.6 ± 3.2
9	43.5 ± 0.2	17.1 ± 0.1
10	31.5 ± 5.8	60.8 ± 6.2
11	47.7 ± 11.4	132.8 ± 16.2
12	14.5 ± 7.5	35.4 ± 8.6
13	41.7 ± 8.2	214.9 ± 15.2
14	15.3 ± 3.1	24.3 ± 3.4
Gefitinib	18.2 ± 2.2	368.2 ± 25.6
Osimertinib	57.8 ± 10.2	8.5 ± 2.7

simulation approach were elucidated secondarily by docking **erlotinib** and **TAK-285** as the co-localized ligands at the active sites of both $EGFR^{WT}$ and $EGFR^{T790M}$. The root mean square deviation (RMSD) values of **erlotinib** and **TAK-285** secondly docked analogs and co-localized conformers, respectively, were 1.4 and 1.85 Å, respectively, illustrating the rationality of this docking technique (Fig. 1S and 5S, respectively, in ESI†).

To investigate the potential dual EGFR inhibitory activities of **gefitinib** and **osimertinib**, these reversible first- and irreversible third-generation EGFR inhibitors were docked against wild-type and mutant EGFR, respectively. Additionally, **erlotinib**, the co-localized ligand, was re-docked into its corresponding co-crystalized protein model (PDB code: 4HJO) to evaluate the ability of MOE to replicate the native ligand superimposition to the wild-type EGFR protein active site (Fig. 1S and 2S,† and Table 3).

The re-docked **erlotinib** structure exhibited a high degree of similarity with the native ligand, with an energy score (ΔG) of -6.83 kcal mol^{-1} and a good RMSD value of 1.4 Å. Particularly, the re-docked **erlotinib** structure formed one H-bond (hydrogen bond) with Met769 and two H_2O-dependent H-bonds with Gln767 and Thr766, highlighting the accuracy of the docking protocol.

Osimertinib and **gefitinib**, their binding interactions with the active $EGFR^{WT}$ binding site were investigated through molecular docking studies. **Osimertinib** was found to form one π–H bond with Val702, and one π–cation contact with Lys692 AAs (amino acids), resulting in an energy score (ΔG) of -7.01 kcal mol^{-1} and 2.38 Å as its RMSD value (Fig. 3S† and Table 3). However, these interactions were not sufficient to inhibit the $EGFR^{WT}$ protein kinase, consistent with previous literature data indicating that **osimertinib** has a higher affinity for the mutant $EGFR^{T790M}$ protein kinase and no activity against the $EGFR^{WT}$.

In contrast, **gefitinib** was found to form hydrogen bonds with Met769 and H_2O-assisted H-bonds with Thr766 and Gln767 amino acids, similar to **erlotinib**. Additionally, **gefitinib** formed two hydrophobic bonds with Leu694 and Leu820 AAs within the EGFR binding site, resulting in an energy score (ΔG) of -8.01 kcal mol^{-1} and an RMSD value of 1.33 Å (Fig. 4S† and Table 3). These interactions suggest that **gefitinib** can afford good inhibitory activity within the $EGFR^{WT}$ protein active site, consistent with its use as reference drug in the *in vitro* experiments.

Derivatives **5**, **12**, and **14**, their binding interactions with the active $EGFR^{WT}$ binding site (PDB code: 4HJO) were investigated. Derivative **5** was able to bind to the $EGFR^{WT}$ active site with a satisfactory interaction affinity, exhibiting an energy score (ΔG) of -6.40 kcal mol^{-1} and 1.99 Å as its RMSD value. The binding mode of derivative **5** involved one H bond with Lys721 AA and one π–H bond with the major amino acid Met769 (Fig. 4 and Table 3). Derivative **12** demonstrated a good interaction affinity relative to the reference **erlotinib**, with an energy score (ΔG) of -7.10 kcal mol^{-1} and 1.05 Å as its RMSD value (Fig. 5 and Table 3). The binding mode of derivative **12** involved hydrogen bonds with Met769, Lys692, Lys704, and H_2O-assisted H-bonds with Thr766 and Gln767 amino acids, similar to **erlotinib**. Additionally, derivative **12** formed two hydrophobic bonds with Val702 amino acid within the EGFR binding site. Derivative **14** exhibited a different binding mode than **erlotinib**, with an acceptable interaction affinity relative to **erlotinib**, characterized by an energy score (ΔG) of -6.53 kcal mol^{-1} and 2.14 Å as its RMSD value (Fig. 6 and Table 3). The binding interaction mode of derivative **14** involved a H-bond with the

Table 3 Molecular docking results for **8**, **12**, **14**, **erlotinib**, **gefitinib**, and **osimertinib** at the main binding site of $EGFR^{WT}$

Comp.	ΔG score kcal mol^{-1}	RMSD_refine (Å)	Amino acid/bond	Distance (Å)	E (kcal mol^{-1})
8	−6.40	1.99	Met769/pi–H	3.98	−0.5
			Lys721/H acceptor	3.39	−2.5
12	−7.10	1.05	Met769/H acceptor	3.34	−1.5
			Lys692/H acceptor	3.21	−1.4
			Lys704/H acceptor	2.95	−8.3
			Val702/pi–H	4.11	−0.5
			Val702/pi–H	4.24	−0.7
			HOH Thr766/H acceptor	3.17	−0.7
			HOH Gln767/H acceptor	3.17	−0.7
14	−6.53	2.14	Met769/H donor	2.98	−0.6
			Lys721/H acceptor	2.91	−8.1
			Leu694/pi–H	3.91	−0.7
			Val702/pi–H	3.84	−0.8
Erlotinib	−6.83	1.4	Met769/H acceptor	2.95	−4.4
			HOH Thr766/H donor	3.03	−1.6
			HOH Gln767/H donor		−1.1
Gefitinib	−8.01	1.33	Met769/H acceptor	3.03	−3.3
			HOH Thr766/H donor	3.10	−1.5
			HOH Gln767/H donor	3.10	−1.5
			Leu694/pi–H	4.3	−0.8
			Leu820/pi–H	4.56	−0.7
Osimertinib	−7.01	2.38	Lys692/pi–cation	4.38	−0.7
			Val702/pi–H	3.77	−0.7

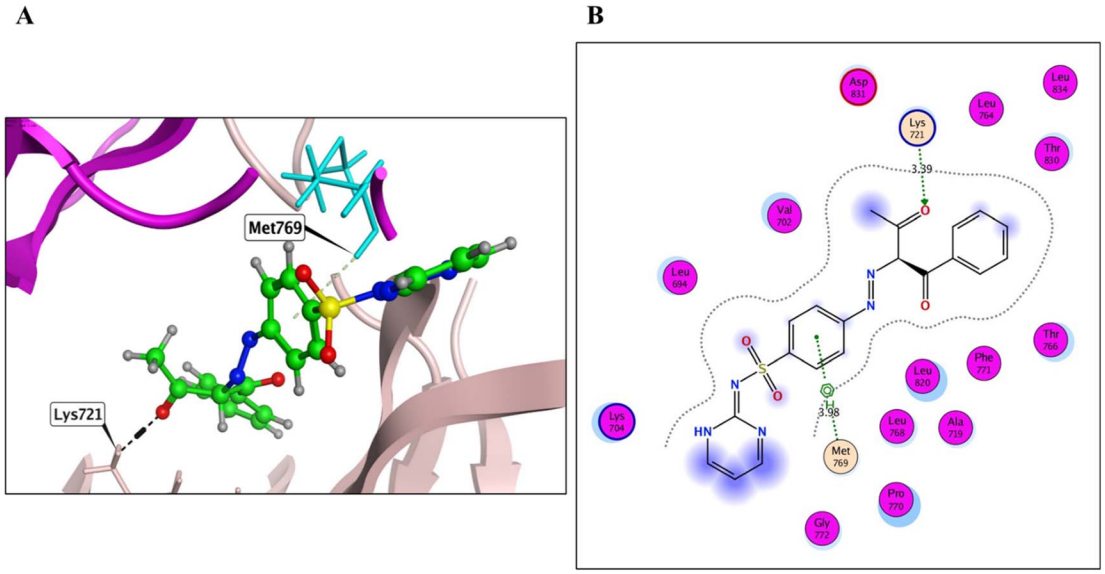

Fig. 4 3D (A) and 2D images (B) of **8** (green sticks) within the wild EGFR kinase.

major amino acid Met769 and another hydrogen bond with Lys721 AA inside the $EGFR^{WT}$ active site. Furthermore, derivative **14** formed two hydrophobic interactions with Leu694 and Val702 AAs.

The binding interactions of derivatives **8**, **12**, and **14** with the $EGFR^{T790M}$ mutant model (PDB code: 3W2O) were investigated and the outcomes illustrated that these derivatives displayed good binding affinities *versus* $EGFR^{T790M}$, with energy scores ranging from −6.33 to −7.53 kcal mol^{-1} (Table 4). Relying on previous literature data about the $EGFR^{T790M}$ mutant model, Met790 amino acid in the $EGFR^{T790M}$ mutant model can adopt specific conformations to fit with various inhibitors, while the R858 residue can afford conformational activation loop variants. These outcomes provide a deeper understanding of the SARs that can facilitate the development of more efficient inhibitory agents against sensitive and resistant drug-dependent EGFR mutations.[51] Regarding the validation of the docking protocol of the co-crystallized ligand **TAK-285**, we re-docked it into its corresponding $EGFR^{T790M}$ adenine binding pocket of the co-crystal protein model (PDB code: 3W2O). The results showed that the re-docked **TAK-285** binding score (ΔG) was −7.35 kcal mol^{-1}, with a good RMSD value of 3.01 Å (Fig. 5S† and Table 4). The binding mode of **TAK-285** involved one H-bond with each Met793, Asp800, Leu788, and Lys745 amino acids. Additionally, the pyrimidine ring of **TAK-285** formed one H_2O-assisted H-bond with Met790, with 3.01 Å as the bond length value.

The binding interactions of **gefitinib**, **osimertinib**, and **erlotinib** with the $EGFR^{T790M}$ mutant model (PDB code: 3W2O) were investigated as well. **Gefitinib**, utilized as a reference in the *in vitro* experiments, was found to form only one significant hydrogen bond with Met790 AA, with 3.62 Å a distance value and an energy score of −5.98 kcal mol^{-1} (Fig. 6S† and Table 4). In contrast, **osimertinib** was found to bind to the $EGFR^{T790M}$

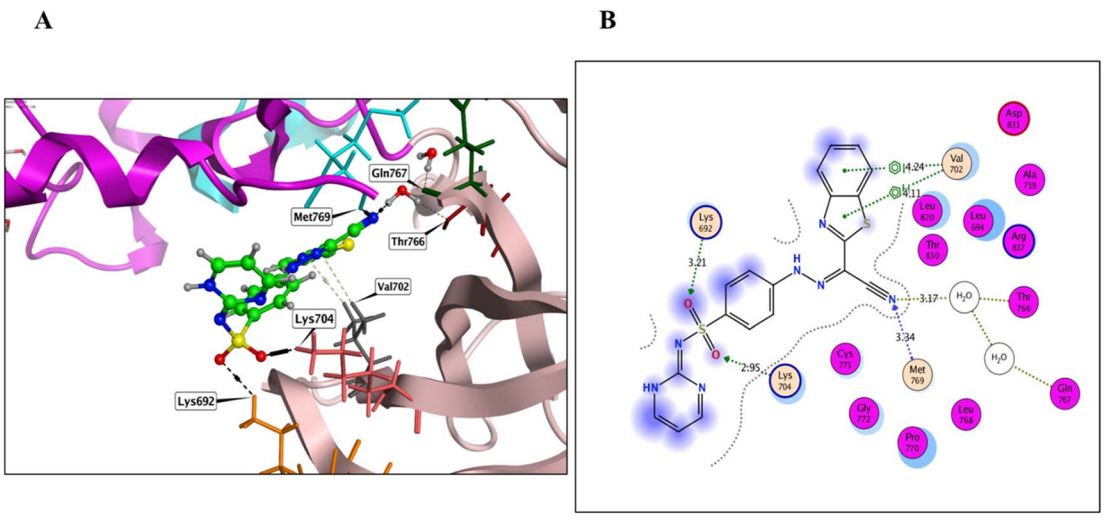

Fig. 5 3D (A) and 2D images (B) of **12** (green sticks) within the wild EGFR kinase.

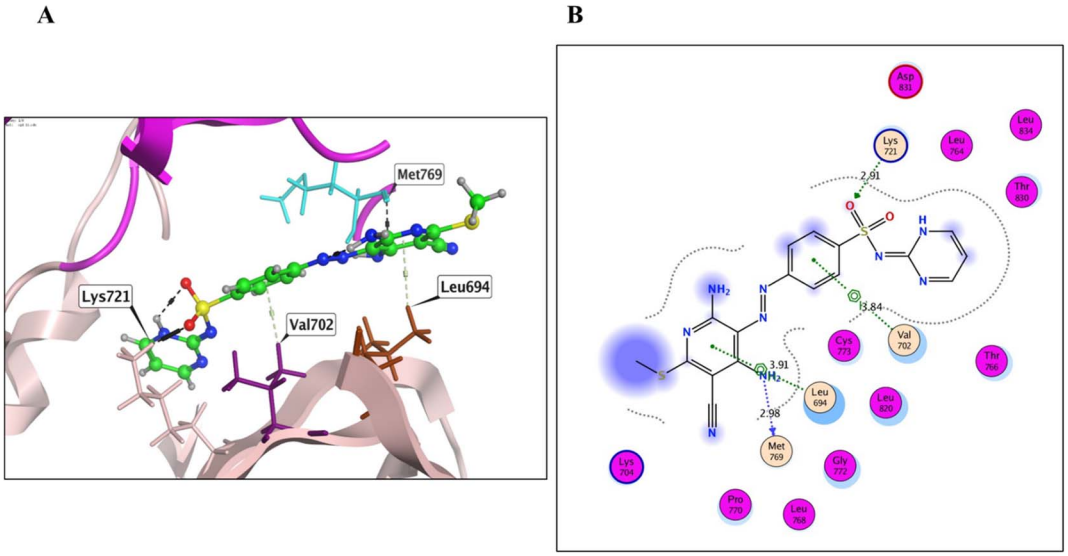

Fig. 6 3D (A) and 2D images (B) of **14** (green sticks) within the wild EGFR kinase.

mutant model in a more potent manner, with a binding score (ΔG) of −8.72 kcal mol^{-1} and an RMSD value of 1.53 Å (Fig. 7S† and Table 4). The binding mode of **osimertinib** involved two H-bonds with Met790, one H-bond with Glu762, two ionic bonds with Asp855, and three hydrophobic bonds with Leu718 AA within the mutant EGFR^{T790M} binding site. These results suggest that **osimertinib** can afford potent inhibitory activity within the mutant EGFR^{T790M} protein active site, consistent with its auspicious IC_{50} value in the *in vitro* EGFR^{T790M} biological investigation. **Erlotinib** was also re-docked against the mutant EGFR^{T790M} binding site to evaluate its affinity. The results elucidated that **erlotinib** made H-bonds with only two non-essential amino acids, Met769 and Lys745, with distances of 3.84 and 3.04 Å, respectively (energy score = −6.54 kcal mol^{-1}) (Fig. 8S† and Table 4). These findings are consistent with literature data, which suggest that **erlotinib** has

Table 4 Molecular modelling results for **8**, **12**, **14**, **gefitinib**, **Tak-285**, **erlotinib**, and **osimertinib** at the active binding site of mutant EGFR^{T790M}

Comp.	ΔG score kcal mol^{-1}	RMSD-refine (Å)	Amino acid/bond	Distance (Å)	E (kcal mol^{-1})
8	−7.53	2.03	Met790/H donor	3.56	−0.9
			Gly796/H acceptor	3.38	−0.5
			Gly796/H acceptor	3.46	−0.5
12	−6.62	1.73	Met790/H donor	4.15	−0.5
			Ile752/H donor	4.30	−0.7
			Val726/pi–H	4.37	−0.7
			HOH Met790/H acceptor	2.93	−0.8
14	−6.33	1.06	HOH Met790/H acceptor	2.79	−0.8
			Asp855/H donor	2.99	−1.3
Gefitinib	−5.98	1.25	Met790/H donor	3.62	−0.5
TAK-285	−7.35	1.85	HOH Met790/H acceptor	3.01	−0.8
			Met793/H acceptor	3.25	−3.1
			Asp800/H donor	3.10	−2.3
			Leu788/H donor	3.39	−1.3
			Lys745/H acceptor	3.17	−0.8
Osimertinib	−8.72	1.53	Met790/H donor	3.81	−1.1
			HOH Met790/H acceptor	3.31	−0.9
			Glu762/H donor	3.24	−0.7
			Asp855/ionic	3.90	−0.7
			Asp855/ionic	3.81	−0.9
			Leu718/pi–H	4.39	−0.5
			Leu718/pi–H	4.34	−0.5
			Leu718/pi–H	3.96	−1.0
Erlotinib	−6.54	2.06	Met769/H donor	3.84	−0.5
			Lys745/H acceptor	3.04	−4.9

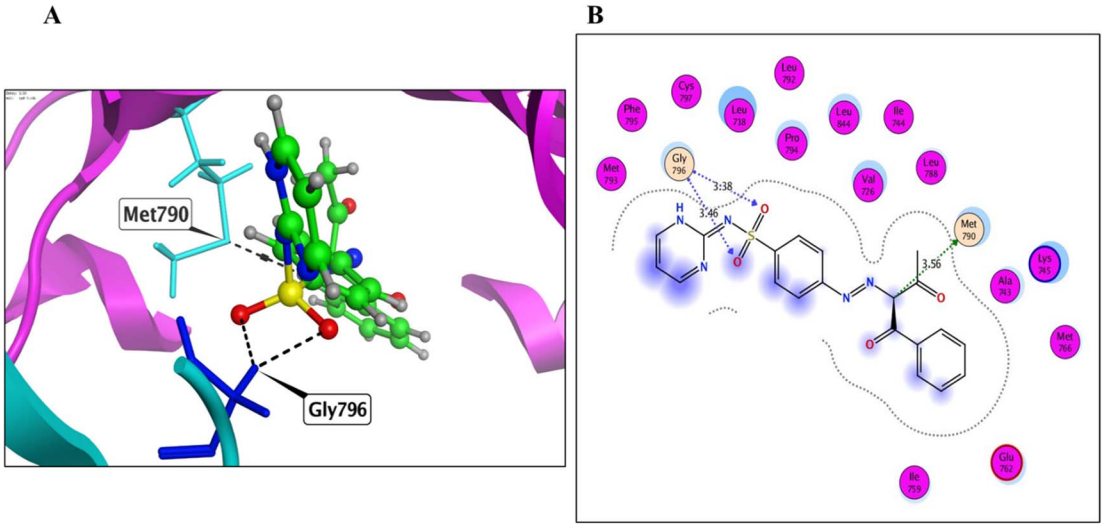

Fig. 7 3D (A) and 2D images (B) of **8** (green sticks) within the mutant EGFR^{T790M} kinase.

affinity only for the wild-type EGFR protein tyrosine kinase, not the mutant EGFR^{T790M} [50].

Derivative **8** was found to bind to the active EGFR^{T790M} site *via* three main H-bonds: one with Met790 and two with Gly796 AAs, with distance values of 3.56, 3.38, and 3.46 Å, respectively (energy score = −7.53 kcal mol^{-1}) (Fig. 7 and Table 4). This binding mode suggests that derivative **8** has a strong affinity for the EGFR^{T790M} mutant model. Derivative **12** was found to bind to the EGFR^{T790M} mutant model in a similar manner to **TAK-285**, with a binding mechanism that involved hydrogen bonding with only two essential amino acids, Met790 and Ile752, with distance values of 4.15 and 4.30 Å (energy score = −6.62 kcal mol^{-1}) (Fig. 8 and Table 4). Additionally, derivative **12** formed one hydrophobic interaction with Val726. Derivative **14** was found to bind to the EGFR^{T790M} mutant model *via* two fundamental H-bonds with Met790 and Asp855, with distance values of 2.79 and 2.99 Å, respectively (energy score = −5.51 kcal mol^{-1}) (Fig. 9 and Table 4). These binding modes highlight the significance of the hydrogen bond donating and accepting moieties in the designed ligands to act as efficient dual EGFR^{WT} and EGFR^{T790M} inhibitors. The results suggest that the designed ligands have the potential to dually inhibit EGFR^{WT} and EGFR^{T790M} protein tyrosine kinases, which is a critical aspect of cancer therapy.

3.2. Structure–activity relationship (SAR) study

Our rationalized drug design approach involved a comprehensive study of SAR of the target derivatives as potential antiproliferative agents. Specifically, we investigated the impact of R_1 and R_2 substituents on the biological activity of the scaffolds (Fig. 10). The results of our study revealed that compounds **8**, **12**, and **14** exhibited highly potent IC_{50} values, indicating significant *in vitro*

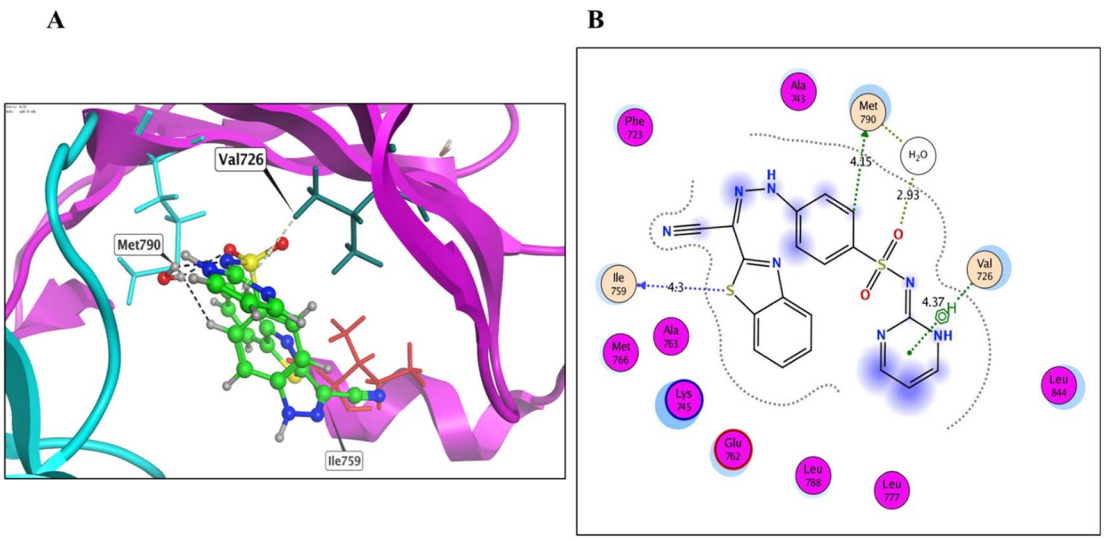

Fig. 8 3D (A) and 2D images (B) of **12** (green sticks) within the mutant EGFR^{T790M} kinase.

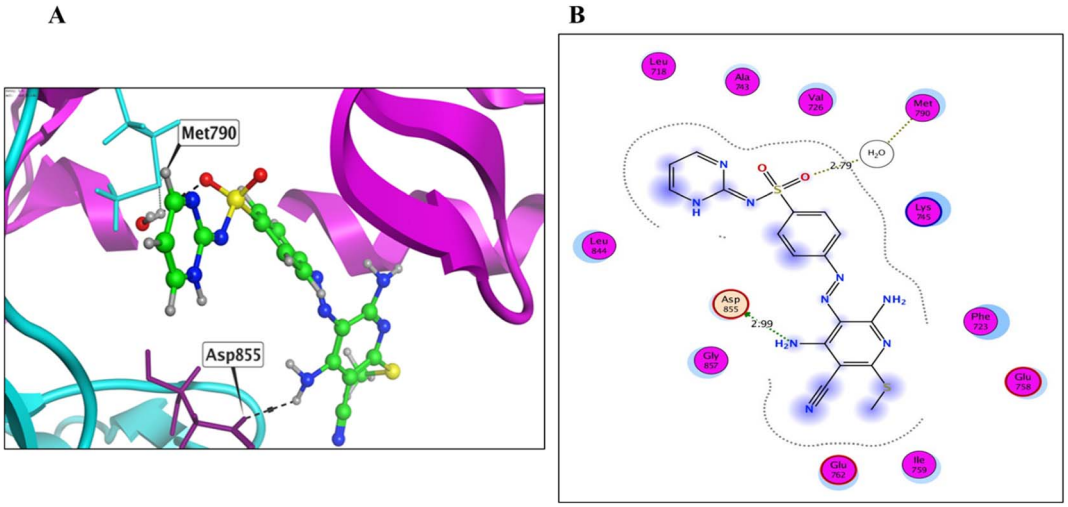

Fig. 9 3D (A) and 2D images (B) of **14** (green sticks) within the mutant EGFR^{T790M} kinase.

antiproliferative activities and dual EGFR^{WT} and EGFR^{T790M} inhibitory activity. Furthermore, molecular docking studies demonstrated that these compounds formed strong interactions with the target protein, which correlated with their high biological activity. A key finding of our SAR analysis was the importance of hydrogen bond acceptor (HBA) functional groups in achieving effective dual EGFR inhibition. The presence of HBA groups in compounds **8**, **12**, and **14** was found to be crucial for their outstanding potency and selectivity towards both EGFR^{WT} and EGFR^{T790M}. These results afford valuable information that greatly helps in the design of novel EGFRIs and illustrate the importance of careful consideration of the SAR of target compounds in the production of promising cancer therapies.

Lapatinib has been shown to interact with the inactive tyrosine kinase domain of EGFR due to its large, sterically hindered [(3-fluorobenzyl)oxy] core scaffold on the peripheral aniline

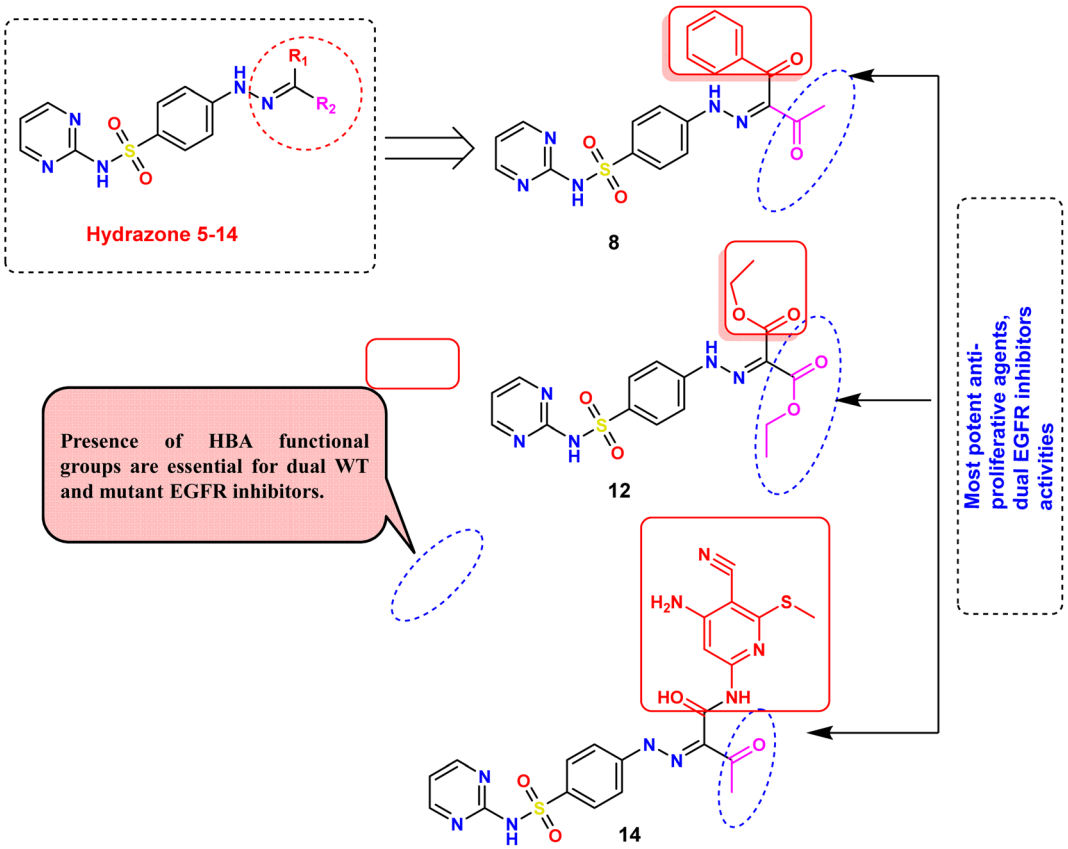

Fig. 10 SAR study of sulfadiazine-based hydrazones **8**, **12**, and **14**.

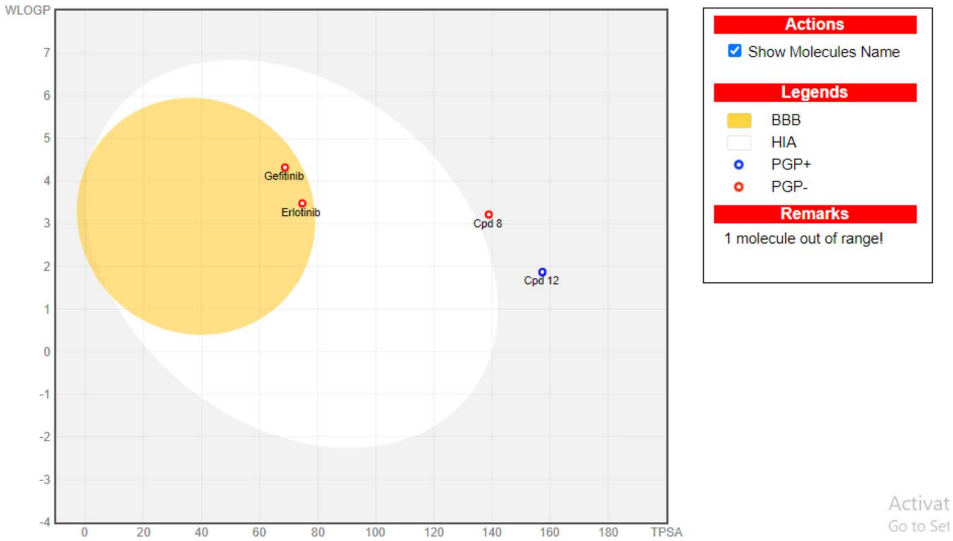

Fig. 11 The boiled-egg diagram for **8**, **12**, **14**, **erlotinib**, and **gefitinib**.

residue. This prevents it from fitting into the small-sized ATP-binding site, instead allowing it to reach and fit into the allosteric-binding site that is re-opened by the dislocation of the αC helix in the inactive conformation model.[52] Similarly, the large-sized R_1 and R_2 side chains in compounds **8**, **12**, and **14**, particularly in compound **12**, prevent them from fitting into the small ATP-binding pocket. As a result, compound **12** selectively interacts with the inactive EGFR conformation, but not the active one. Compound **12** was detected to be the most active inhibitor of both $EGFR^{WT}$ and $EGFR^{T790M}$ kinases among all tested derivatives. This is attributed to its binding mode, dimensions, and stable docking scores, which are superior to those of the reference inhibitors **erlotinib** and **gefitinib** for wild-type EGFR, and **TAK-285** and **osimertinib** for mutant $EGFR^{T790M}$. These outcomes are coherent with the *in vitro* inhibition of compound **12** against both $EGFR^{WT}$ and $EGFR^{T790M}$ protein kinases, demonstrating its potential as a potent and selective EGFR inhibitor.

3.3. Pharmacokinetic characteristics and ADMET predict

To further investigate the potential of the synthesized scaffolds as orally bioavailable candidates,[52] their absorption, distribution, metabolism, and excretion (ADME) properties were evaluated using the ADME Swiss prediction free online tool.[51–56] The boiled egg diagram of the WLOGP *versus* TPSA (Topological Polar Surface Area) of the uploaded derivatives **8** and **12** revealed that both compounds have low GI absorption and are unable to pass through the BBB relative to the reference compounds **erlotinib** and **gefitinib** (Fig. 11). This suggests that these compounds are unlikely to cause central nervous system (CNS) negative impacts due to their low BBB permeability. In contrast, scaffold **14**, a highly polar compound, was found to be out of range and vanished from the boiled egg diagram, highlighting the need for optimization to make it an effective orally bioavailable candidate. The ADME Swiss prediction tool also suggested that derivative **8** is unlikely to be a P-glycoprotein (PGP) substrate, which means that it may not be exposed to drug resistance mechanisms. However, scaffold **12** is predicted to be a PGP substrate, indicating a possibility of exposure to drug resistance mechanisms. The TPSA values of the designed scaffolds **8**, **12**, and **14** ranged from 138 to 216.04 $Å^2$, while their log *P* values were between 1.85 and 3.93 (Table 5). These values provide further insight into the lipophilicity and bio-molecular polarity of the designed scaffolds.

The bioavailability diagram for scaffolds **8**, **12**, and **14** is displayed in Fig. 12(A–E). This radar plot consists of six axes representing six critical oral bioavailability characteristics: solubility (INSOLU), flexibility (FLEX), size (SIZE), lipophilicity (LIPO), saturation (INSATU), and polarity (POLAR) (Table S1†). The pink area in the radar plot represents the optimum property parameters for oral bioavailability. The red colored lines represent scaffolds **8** (Fig. 12A), **12** (Fig. 12B), and **14** (Fig. 12C), which are nearly within the pink area relative to **erlotinib** (Fig. 12D) and **gefitinib** (Fig. 12E). This suggests that the designed scaffolds have acceptable assumed oral

Table 5 ADMET outcomes of **8**, **12**, **14**, and **erlotinib** and **gefitinib** *via* Swiss ADME webserver

Comp.	M. wt	Fraction Csp^3	RB	HBA	HBD	MR	TPSA	Log *P*	GI absorption	BBB perm.	Lip. V.	Bio. Sc.
8	423.45	0.05	8	7	2	111.67	138.86	3.22	Low	No	Yes	0.55
12	435.48	0.00	6	7	2	114.36	169.64	3.93	Low	No	Yes	0.55
14	441.49	0.06	6	8	4	119.04	216.04	1.85	Low	No	Yes	0.55
Erlotinib	393.44	0.27	10	6	1	111.40	74.73	3.07	High	Yes	Yes	0.55
Gefitinib	446.90	0.36	8	7	1	121.66	68.74	4.32	High	Yes	Yes	0.55

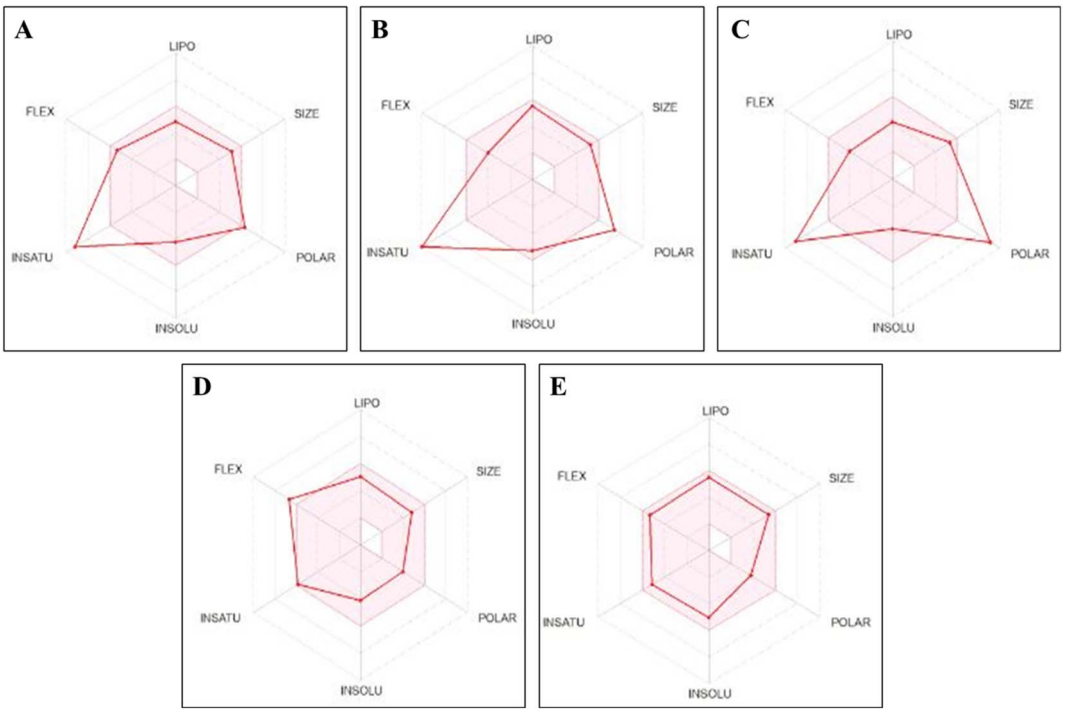

Fig. 12 Pink zoned oral bioavailability radars for **8** (A), **12** (B), **14** (C), **erlotinib** (D), and **gefitinib** (E).

bioavailability. Scaffolds **8**, **12**, and **14** are predicted to afford a suitable bioavailability with a score value equal to 0.55, similar to the reference compounds **erlotinib** and **gefitinib**. Additionally, scaffolds **8** and **12** follow the Lipinski rule of 5 with no detected violations, similar to the reference drugs. However, derivative **14** obeys the Lipinski rule of 5 with only one detected violation (number of polar atoms; nitrogen or oxygen atoms higher than 10) compared to the reference compounds (Table S1†). These results demonstrate that the designed compounds have promising pharmacokinetic and drug-like properties. As shown in Fig. 12(A–E) and Table 5, analogs **8** and **12** have good lipophilic characters compared to the reference compounds, unlike compound **14**, which has lower lipophilicity. The unsaturation property of scaffolds **8**, **12**, and **14** is nearly out of the tinted area, indicating that these compounds may require optimization to improve their saturation characteristics. The fraction Csp^3 values of scaffolds **8**, **12**, and **14** were calculated at 0.06, indicating that these compounds have a low ratio of sp^3 hybridized carbons over all the carbon numbers. For saturation character, the ratio of sp^3 hybridized carbons over all the carbon numbers of the analog (fraction Csp^3) should not be lower than 0.25.

Hydrazones **8**, **12**, and **14** exhibited low saturation character, with fraction Csp^3 values of 0.05, 0.00, and 0.06, respectively. Conversely, their hydrophilicity ranged from moderately soluble to very soluble, relative to the reference compounds **erlotinib** and **gefitinib**, which had solubility ranging from moderately soluble to poorly soluble. Unlike **erlotinib** and **gefitinib**, which showed inhibitory activity against CYP2C9, CYP2C19, CYP2D6, and CYP3A4, hydrazones **8**, **12**, and **14** did not exhibit inhibitory activity against CYP1A2 and CYP2D6. Additionally, scaffold **14** did not show inhibitory activity against CYP2C9 and CYP2C19, unlike derivatives **8** and **12**. According to PAINS and Brenk filters, hydrazones **8**, **12**, and **14** are suitable for biological experiments, exhibiting potent chemical reactivity, low hazardous doses, and adequate metabolic stability. Scaffolds **8**, **12**, and **14** demonstrated lead-likeness, unlike **erlotinib** and **gefitinib**, and their synthetic procedures were categorized as accessible. Compounds **8**, **12**, and **14** had better safety profiles than the reference compounds **erlotinib** and **gefitinib** (Table S1†). These compounds are classified as non-AMES toxic, hERG I inhibitors, and skin sensitization agents. Hydrazones **8**, **12**, and **14** exhibited hepatotoxicity and parameters indicating carcinogenic agents, which may cause severe hepatic side effects, similar to the reference compounds **erlotinib** and **gefitinib**. Compounds **8** and **12** demonstrated hERG II K^+ channel inhibitory activity, similar to the reference compounds **erlotinib** and **gefitinib**. In contrast, scaffold **14** did not exhibit hERG II K^+ channel inhibitory activity (Table S1†).

4. Experimental part

4.1. General chemistry

All general information were provided in the ESI.†

4.2. Synthesis of sulfadiazine 4

A mixture of an equimolar amount of 4-acetamidobenzene sulfonyl chloride (**1**) with 2-aminopyrimidine (**2**) was refluxed in pyridine for 1 hour, then the mixture was added to 5 mL of H_2O/HCl in ratio 2 : 1, then filtered the mixture, washed with H_2O several times, dried, and recrystallized from EtOH, m.p. 251–253 °C (reported m.p. 252–256 °C).[37]

4.3. Synthesis of sulfadiazine 5–14

A solution of sodium nitrite (0.1 g, 1.3 mmol) in water (2 mL) was gradually added to a solution of sulfadiazine (0.25 g, 1 mmol) in conc. HCl (3 mL) at 0–5 °C. The formed diazonium was mixed under stirring with an ice-cooled solution of appropriate coupling compounds (1 mmol), namely, ethyl acetoacetate, acetylacetone, ethyl benzoylacetate, benzoyl acetone, ethyl cyanoacetate, cyanothioacetamide, dimer of malononitrile, diethyl malonate, *N*-[4-amino-5-cyano-6-(methylthio)pyridin-2-yl]-3-oxobutanamide and 4,6-diamino-2-(methylthio)nicotinonitrile in pyridine (20 mL). The mixture was kept for 30 minutes in an ice bath and then mixed into 100 mL of cold water. The product was filtered off, washed with distilled water, dried, and recrystallized from EtOH.

4.3.1. 4-(2-(2,4-Dioxohexan-3-ylidene)hydrazineyl)-*N*-(pyrimidin-2-yl)benzenesulfonamide (5).

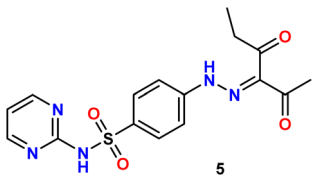

5

Brownish yellow solid, yield (91%), m.p. 160–162 °C. IR (KBr) ν: 3404, 3256 (2NH), 3089, 3039 (C–H Aromatic), 2974, 2938, 2874, 2811, 2734 (C–H aliphatic), 1690 (br, C=O), 1584 (C=N); ^{1}H NMR δ: 1.25–1.29 (t, 3H, J = 8 Hz, $CH_{3\ ester}$), 2.41 (s, 3H, C$\underline{H}_3$), 4.29–4.34 (q, 2H, J = 8 Hz, CH_2), 7.03–7.06 (t, 1H, J = 6 Hz, C$\underline{H}_{arom}$), 7.54–7.56 (d, 2H, J = 8 Hz, C$\underline{H}_{arom}$), 7.97–8.00 (d, 2H, J = 12 Hz, C$\underline{H}_{arom}$), 8.50–8.51 (d, 2H, J = 4 Hz, C$\underline{H}_{arom}$), 11.59 (s, 1H, N$\underline{H}$, D_2O exchangeable), 11.76 (br, 1H, N$\underline{H}$, D_2O exchangeable); ^{13}C NMR δ: 14.28 ($CH_{3\ ester}$), 25.76 (CH_3), 61.84 (CH_2), 115.06, 116.21, 129.97, 134.22, 134.62, 146.55, 157.44, 158.75, 162.60 (C=O), 194.31 (C=O); anal. calcd for $C_{16}H_{17}N_5O_5S$ (391.40): C, 49.10; H, 4.38; N, 17.89. Found: C, 49.22; H, 4.26; N, 17.75.

4.3.2. 4-(2-(2,4-Dioxopentan-3-ylidene)hydrazineyl)-*N*-(pyrimidin-2-yl)benzenesulfonamide (6).

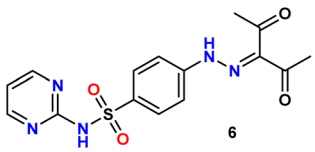

6

Yellow solid, yield (80%), m.p. 228–230 °C. IR ν: 3422, 3312 (2NH), 3082, 3033 (C–H aromatic), 2936, 2865, 2808, 2729 (C–H aliphatic), 1677 (C=O), 1585 (C=N); ^{1}H NMR δ 2.42 (s, 3H, C$\underline{H}_3$), 2.47 (s, 3H, C$\underline{H}_3$), 7.04–7.05 (m, 1H, C$\underline{H}_{arom}$), 7.68–7.70 (d, 2H, J = 8 Hz, C$\underline{H}_{arom}$), 8.00–8.02 (d, 2H, J = 8 Hz, C$\underline{H}_{arom}$), 8.50 (s, 2H, C$\underline{H}_{arom}$), 11.70 (br, 1H, N$\underline{H}$, D_2O exchangeable), 13.51 (s, 1H, N$\underline{H}$, D_2O exchangeable); ^{13}C NMR δ: 26.75 (CH_3), 31.70 (CH_3), 116.25, 129.88, 135.83, 135.95, 145.95, 157.34, 158.83, 159.04, 196.92 (C=O), 197.92 (C=O); anal. calcd for $C_{15}H_{15}N_5O_4S$ (361.37): C, 49.85; H, 4.18; N, 19.38. Found: C, 49.73; H, 4.27; N, 19.51.

4.3.3. Ethyl-3-benzoyl-2-(4-(*N*-(pyrimidin-2-yl)sulfa) hydrazineylidene)propanoate (7).

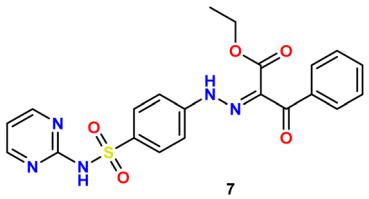

7

Yellow solid, yield (76%), m.p. 205–207 °C; IR ν: 3224, 3172 (2NH), 3083, 3039 (C–H aromatic), 2984, 2942, 2874, 2813, 2738 (C–H aliphatic), 1684, 1662 (C=O), 1582 (C=N); ^{1}H NMR δ: 1.24–1.27 (t, 3H, J = 6 Hz, C$\underline{H}_3$), 4.32–4.37 (q, 2H, J = 6 Hz, C$\underline{H}_2$), 7.01–7.04 (m, 1H, C$\underline{H}_{arom}$), 7.39–7.41 (d, 2H, J = 8 Hz, C$\underline{H}_{arom}$), 7.53–7.60 (m, 3H, C$\underline{H}_{arom}$), 7.65–7.72 (m, 1H, C$\underline{H}_{arom}$), 7.91–7.98 (m, 3H, C$\underline{H}_{arom}$), 7.49–8.51 (m, 2H, C$\underline{H}_{arom}$), 11.66 (br, 1H, N$\underline{H}$), 11.99 (br, 1H, N$\underline{H}$); ^{13}C NMR δ: 14.27 ($CH_{3\ ester}$), 61.91 (CH_2), 115.12, 116.20, 128.28, 129.56, 129.97, 130.37, 133.43, 134.73, 137.04, 146.44, 157.41, 158.76, 162.43 (C=O), 192.49 (C=O); anal. calcd for $C_{21}H_{19}N_5O_5S$ (453.47): C, 55.62; H, 4.22; N, 15.44. Found: C, 55.47; H, 4.38; N, 15.32.

4.3.4. 4-[2-(1-Benzoyl-2-oxopropylidene)hydrazino]-*N*-pyrimidin-2-ylbenzenesulfonamide (8).

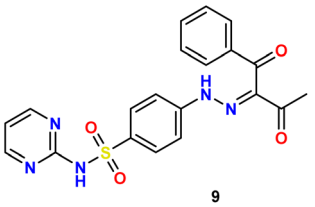

9

Orange solid, yield (75%), m.p. 235–237 °C. IR ν: 3268, 3113 (2NH), 3084, 3038 (C–H aromatic), 2943, 2873, 2813, 2739 (C–H aliphatic), 1655 (C=O), 1582 (C=N); ^{1}H NMR δ 2.51 (s, 3H, CH_3), 7.03–7.05 (t, 1H, J = 4 Hz, C$\underline{H}_{arom}$), 7.50–7.58 (m, 4H, C$\underline{H}_{arom}$), 7.69–7.72 (t, 1H, J = 6 Hz, C$\underline{H}_{arom}$), 7.80–7.82 (d, 2H, J = 8 Hz, C$\underline{H}_{arom}$), 7.95–7.97 (d, 2H, J = 8 Hz, CH_{arom}), 8.50–8.51 (d, 2H, J = 4 Hz, C$\underline{H}_{arom}$), 11.34 (s, 1H, N$\underline{H}$), 13.65 (s, 1H, N$\underline{H}$); ^{13}C NMR δ: 25.39 (CH_3), 114.58, 116.22, 129.21, 129.54, 129.94, 133.84, 134.94, 135.85, 141.45, 147.22, 157.22, 158.77, 195.22 (C=O), 196.65 (C=O); anal. calcd for $C_{20}H_{17}N_5O_4S$ (423.44): C, 56.73; H, 4.05; N, 16.54. Found: C, 56.57; H, 4.21; N, 16.47.

4.3.5. Ethyl (Z)-2-cyano-2-(2-(4-(*N*-(pyrimidin-2-yl) sulfamoyl)phenyl)hydrazineylidene)acetate (9).

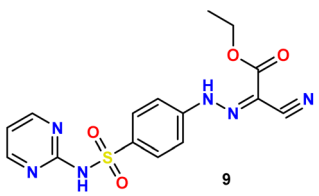

9

Yellow solid, yield (78%), m.p. 225–227 °C; IR ν: 3387, 3218 (2NH), 3036, 3032 (C–H aromatic), 2972, 2935, 2866, 2806 (C–H aliphatic), 2214 (C≡N), 1725 (C=O), 1582 (C=N); ^{1}H NMR δ: 1.27–1.30 (t, 3H, J = 6 Hz, C$\underline{H}_3$), 4.27–4.32 (q, 2H, J = 6 Hz, C$\underline{H}_2$), 7.03–7.06 (t, 1H, J = 6 Hz, C$\underline{H}_{arom}$), 7.59–7.61 (d, 2H, J = 8 Hz, CH_{arom}), 8.01–8.03 (d, 2H, J = 8 Hz, C$\underline{H}_{arom}$), 8.50–8.51 (d, 2H, J = 4 Hz, C$\underline{H}_{arom}$), 11.84 (br, 1H, N$\underline{H}$, D_2O exchangeable) 12.45 (br,

1H, NH, D_2O exchangeable); ^{13}C NMR δ: 14.35 (CH_3), 62.29 (CH_2), 106.78 (C≡N), 111.49, 116.20, 116.64, 129.95, 135.97, 145.81, 157.31, 158.81, 160.89 (C=O); anal. calcd for $C_{15}H_{14}N_6O_4S$ (374.37): C, 48.12; H, 3.77; N, 22.45. Found: C, 48.28; H, 3.63; N, 22.57.

4.3.6. 2-Cyano-(2-(4-(*N*-(pyrimidin-2-yl)sulfamoyl)phenyl) hydrazono)ethanethioamide (10).

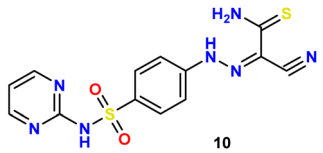

10

Reddish brown solid, yield (69%), m.p. 275–277 °C. IR ν: 3360, 3228, 3188 (NH + NH_2), 3041 (C–H aromatic), 2211 (C≡N), 1581 (C=N); ^1H NMR δ: 7.06–7.08 (t, 1H, J = 4 Hz, C$\underline{H}_{arom}$), 7.86–7.88 (d, 2H, J = 8 Hz, C$\underline{H}_{arom}$), 7.93–7.95 (d, 2H, J = 8 Hz, CH_{arom}), 8.51–8.52 (d, 2H, J = 4 Hz, C$\underline{H}_{arom}$), 9.50 (s, 1H, N$\underline{H}_2$, D_2O exchangeable), 9.87 (s, 1H, N$\underline{H}_2$, D_2O exchangeable), 11.82 (br, 1H, N$\underline{H}$, D_2O exchangeable); ^{13}C NMR δ: 111.30 (C≡N), 115.28, 116.31, 116.52, 129.49, 135.25, 146.12, 157.36, 158.86, 188.03 (C=S); anal. calcd for $C_{13}H_{11}N_7O_2S_2$ (361.40): C, 43.20; H, 3.07; N, 27.13. Found: C, 43.32; H, 3.19; N, 27.02.

4.3.7. 2-Amino-3,3-dicyano-*N*-(4-(*N*-(pyrimidin-2-yl) sulfamoyl)phenyl)acrylohydrazonoyl cyanide (11).

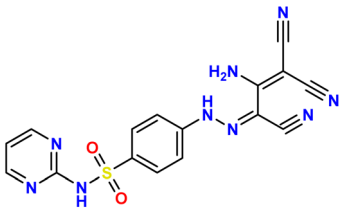

11

Yellow solid, yield (77%), m.p. 295–297 °C; IR ν: 3370, 3303, 3214 (NH + NH_2), 3088, 3050 (C–H aromatic), 2215 (br, C≡N), 1634 (C=N); ^1H NMR δ: 7.06–7.09 (t, 1H, J = 4 Hz, C$\underline{H}_{arom}$), 7.53 (br, 1H, N$\underline{H}$), 7.76–7.78 (d, 2H, J = 8 Hz, C$\underline{H}_{arom}$), 8.22–8.24 (d, 2H, J = 8 Hz, C$\underline{H}_{arom}$), 8.54–8.55 (d, 2H, J = 4 Hz, C$\underline{H}_{arom}$), 10.04 (br, 3H, NH + NH_2); ^{13}C NMR δ: 79.43 (C–$(CN)_2$), 112.91 (C≡N), 114.48 (C≡N), 116.02, 117.29 (C≡N), 127.46. 129.05, 141.51, 144.12, 148.59, 152.58, 157.35, 158.78; anal. calcd for $C_{16}H_{11}N_9O_2S$ (393.38): C, 48.85; H, 2.82; N, 32.05. Found: C, 48.72; H, 2.67; N, 32.22.

4.3.8. Diethyl 2-(2-(4-(*N*-(pyrimidin-2-yl)sulfamoyl)phenyl) hydrazineylidene)malonate (12).

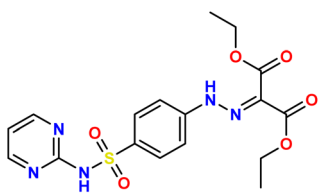

12

Brownish red solid, yield (72%), m.p. 148–150 °C. IR ν: 3225, 3103 (2NH), 3077, 3034 (C–H aromatic), 2981, 2934, 2870, 2806, 2732 (C–H aliphatic), 1722, 1681 (C=O), 1578 (C=N); ^1H NMR δ: 1.25–1.30 (m, 6H, 2C$\underline{H}_3$), 4.23–4.35 (qq, 4H, J = 6.6 Hz, $2CH_2$), 7.02–7.04 (t, 1H, J = 4 Hz, C$\underline{H}_{arom}$), 7.50–7.52 (d, 2H, J = 8 Hz, CH_{arom}), 7.98–8.00 (d, 2H, J = 8 Hz, CH_{arom}), 8.50–8.51 (d, 2H, J = 4 Hz, CH_{arom}), 11.71 (s, 1H, N$\underline{H}$), 11.89 (s, 1H, N$\underline{H}$); ^{13}C NMR δ: 14.33 (CH_3), 14.46 (CH_3), 61.54 (CH_2), 62.01 (CH_2), 115.06, 116.20, 125.15, 129.98, 134.75, 146.34, 157.40, 158.75, 161.69 (C=O), 162.52 (C=O); anal. calcd for $C_{17}H_{19}N_5O_6S$ (421.42): C, 48.45; H, 4.54; N, 16.62. Found: C, 48.59; H, 4.41; N, 16.53.

4.3.9. 4-{-2-[4-Amino-5-cyano-2-imino-6-(methylthio)pyridin-3(2*H*)-ylidene]hydrazino}-*N*-pyrimidin-2-ylbenzenesulfonamide (13).

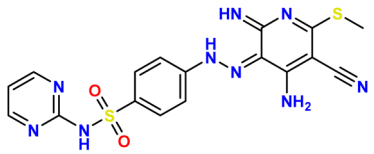

13

Orange solid, yield (80%), m.p. 298–300 °C. IR ν: 3457, 3302, 3205 (NH + NH_2), 3075, 3027 (C–H aromatic), 2935, 2867, 2812, 2734 (C–H aliphatic), 2215 (C≡N), 1574 (C=N); ^1H δ 2.57 (s, 3H, C$\underline{H}_3$), 7.08 (s, 1H, C$\underline{H}_{arom}$), 7.03–7.19 (m, 6H, 4C$\underline{H}_{arom}$ + N$\underline{H}_2$, D_2O exchangeable), 8.52–8.53 (m, 3H, $2CH_{arom}$+ N$\underline{H}$, D_2O exchangeable), 9.19 (br, 1H, NH), 11.91 (br, 1H, N$\underline{H}$, D_2O exchangeable), 13.37 (s, 1H, N$\underline{H}$, D_2O exchangeable); ^{13}C NMR δ: 12.87 (CH_3), 79.92 (C–CN), 114.59, 116.16 (2C), 122.51, 129.08, 139.92, 153.79, 154.48, 155.11, 157.32, 158.88, 168.04; anal. calcd for $C_{17}H_{15}N_9O_2S_2$ (441.49): C, 46.25; H, 3.42; N, 28.55. Found: C, 46.38; H, 3.54; N, 28.41.

4.3.10. *N*-(4-Amino-5-cyano-6-(methylthio)pyridin-2-yl)-3-oxo-2-{[4-(pyrimidin-2-ylsulfamoyl) phenyl]hydrazono}butanamide (14).

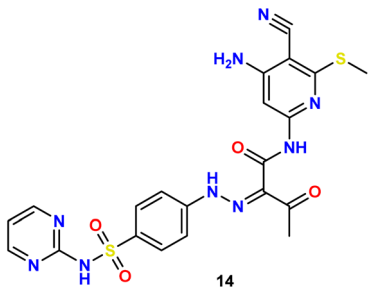

14

Yellow solid, yield (83%), m.p. > 300 °C, IR ν: 3415, 3386, 3341 (NH + NH_2), 3039 (C–H aromatic), 2930, 2871, 2816, 2734 (C–H aliphatic), 2208 (C≡N), 1668 (br, C=O), 1582 (C=N); ^1H NMR δ: 2.52 (s, 3H, C$\underline{H}_3$), 7.06–7.09 (t, 1H, J = 4 Hz, C$\underline{H}_{arom}$), 7.19 (br, 2H, N$\underline{H}_2$), 7.38 (s, 1H, C$\underline{H}_{pyridyl}$), 7.65–7.67 (d, 2H, J = 8 Hz, C$\underline{H}_{arom}$), 8.01–8.03 (d, 2H, J = 8 Hz, C$\underline{H}_{arom}$), 8.52–8.53 (d, 2H, J = 4 Hz, C$\underline{H}_{arom}$), 11.38 (s, 1H, N$\underline{H}$), 11.82 (br, 1H, N$\underline{H}$), 13.37 (s, 1H, N$\underline{H}$); anal. calcd for $C_{21}H_{19}N_9O_4S_2$ (525.56): C, 47.99; H, 3.64; N, 23.99. Found: C, 48.11; H, 3.51; N, 23.83.

4.4. Biological evaluation

4.4.1. *In vitro* anti-proliferative activities. All procedures were provided in the ESI.†

4.4.2. EGFR^{WT} and EGFR^{T790M} kinase inhibitory assay. All procedures were provided in the ESI.†

4.5. Docking studies and ADMET estimation

All procedures were provided in the ESI.†[57–62]

5. Conclusion

A new series of sulfadiazine (**5–14**) was effectively synthesized *via* diazotization of sulfadiazine with some active methylene compounds. The cytotoxic activity of all products was investigated against A431, A549, and H1975 cancer cell panels *via* the MTT assay technique, utilizing **erlotinib**, **gefitinib**, and **osimertinib** as positive controls. Specifically, compounds **8**, **12**, and **14** were revealed to be the most potent analogs on A431, A549, and H1975 cancer cell panels with the IC_{50} values of (4.12, 4.78, and 2.31 μM), (6.38, 5.15, and 6.12 μM), and (6.15, 7.56, and 4.59 μM) compared to **erlotinib** (IC_{50} = 11.09, 17.50, and 12.86 μM), **gefitinib** (IC_{50} = 9.60, 15.75, and 10.15 μM), and **osimertinib** (IC_{50} = 5.96, NT, and 0.93 μM), respectively. Moreover, compound **12** was the most potent tested one *versus* both EGFR^{WT} and EGFR^{T790M} protein kinases with IC_{50} values of 14.5 and 35.4 nM, respectively, compared to **gefitinib** and **osimertinib** as reference drugs with IC_{50} values of 18.2 and 368.2 nM and 57.8 and 8.5 nM, respectively. The molecular-docking results of scaffolds **8**, **12**, and **14** inside both the EGFR^{WT} and EGFR^{T790M} ATP active sites elucidated their ability to afford the critical fitting interactions made within the kinase domain by the references **erlotinib**, **gefitinib**, and **osimertinib**, respectively. Furthermore, investigating the physicochemical characteristics of the most outstanding EGFR inhibitors, compounds **8**, **12**, and **14**, through the Swiss ADME web server illustrated good GIT absorption, lipophilicity, and low BBB penetration characteristics. The valuable outcomes from this simulation study are that scaffolds **8** and **12** are assumed to be the most promising analogs regarding their dual EGFR^{WT} and EGFR^{T790M} inhibitory activity, as well as promising anti-proliferative lead compounds with good pharmacokinetic properties. These findings suggest that these scaffolds should be further investigated and optimized for more potent and selective antiproliferative activity in the future.

Data availability

All data generated or analyzed during this study are included in this published article (and its ESI†).

Conflicts of interest

The authors declare no conflict of interest.

Acknowledgements

This work was supported by the Deanship of Scientific Research, Vice Presidency for Graduate Studies and Scientific Research, King Faisal University, Saudi Arabia [Grant KFU241525]. The authors are thankful to the Researchers Supporting Project number (RSP2024R516) at King Saud University, Riyadh, Saudi Arabia. The authors would like to thank the Deanship of Scientific Research at Shaqra University for supporting this work.

References

1 L. Kujtan and J. Subramanian, Epidermal growth factor receptor tyrosine kinase inhibitors for the treatment of non-small cell lung cancer, *Expert Rev. Anticancer Ther.*, 2019, **19**(7), 547–559.
2 H. Hayashi, E. Nadal, J. E Gray, A. Ardizzoni, N. Caria, T. Puri and C. Grohe, Overall treatment strategy for patients with metastatic NSCLC with activating EGFR mutations, *Clin. Lung Cancer*, 2022, **23**(1), e69–e82.
3 L. Hu, M. Fan, S. Shi, X. Song, F. Wang, H. He and B. Qi, Dual target inhibitors based on EGFR: Promising anticancer agents for the treatment of cancers, *Eur. J. Med. Chem.*, 2022, **227**, 113963.
4 A. Y. Helena and M. E Arcila, Analysis of tumor specimens at the time of acquired resistance to EGFR-TKI therapy in 155 patients with EGFR-mutant lung cancers, *Clin. Cancer Res.*, 2013, **19**(8), 2240–2247.
5 P. C. C. Lv, F. Zhou and J. Chen, Design, synthesis and biological evaluation of thiazolidinone derivatives as potential EGFR and HER-2 kinase inhibitors, *Bioorg. Med. Chem.*, 2010, **18**(1), 314–329.
6 H. Gourdeau, L. Leblond, B. Hamelin, C. Desputeau, K. Dong, I. Kianicka, D. Custeau, C. Boudreau, L. Geerts and S.-X. Cai, Antivascular and antitumor evaluation of 2-amino-4-(3-bromo-4, 5-dimethoxy-phenyl)-3-cyano-4 H-chromenes, a novel series of anticancer agents, *Mol. Cancer Ther.*, 2004, **3**, 1375–1384.
7 S. Sogabe, Y. Kawakita, S. Igaki, H. Iwata, H. Miki, D. R. Cary, T. Takagi, S. Takagi, Y. Ohta and T. Ishikawa, Structure-Based Approach for the Discovery of Pyrrolo[3,2- d] pyrimidine-Based EGFR T790M/L858R Mutant Inhibitors, *ACS Med. Chem. Lett.*, 2013, **4**, 201–205.
8 J. Xu, J. Wang, S. Zhang, *et al.*, Mechanisms of resistance to irreversible epidermal growth factor receptor tyrosine kinase inhibitors and therapeutic strategies in non-small cell lung cancer, *Oncotarget*, 2017, **8**(52), 90557.
9 M. G. Kumar, S. Arora, G. Joshi, *et al.*, Design and Synthesis of Non-Covalent Imidazo [1, 2-a] quinoxaline-Based Inhibitors of EGFR and Their Anti-Cancer Assessment, *Molecules*, 2021, **26**(5), 1490–1503.
10 A. N. Hata, M. J. Niederst and H. L Archibald, Tumor cells can follow distinct evolutionary paths to become resistant to epidermal growth factor receptor inhibition, *Nat. Med.*, 2016, **22**(3), 262–269.
11 M. O. Aboelez, A. Belal, G. Xiang and X. Ma, Design, synthesis, and molecular docking studies of novel pomalidomide-based PROTACs as potential anti-cancer agents targeting EGFRWT and EGFRT790M, *J. Enzyme Inhib. Med. Chem.*, 2022, **37**, 1196–1211.

12 X. Zhang, F. Xu, L. Tong, *et al.*, Design and synthesis of selective degraders of EGFRL858R/T790M mutant, *Eur. J. Med. Chem.*, 2020, **192**, 112199.
13 M. S. Kamel, A. Belal, M. O. Aboelez, E. K. Shokr, H. Abdel-Ghany, H. S. Mansour, A. M. Shawky and M. A. El-Remaily, Microwave-Assisted Synthesis, Biological Activity Evaluation, Molecular Docking, and ADMET Studies of Some Novel Pyrrolo [2, 3-b] Pyrrole Derivatives, *Molecules*, 2022, **27**(7), 2061.
14 M. E. Shoman, M. O. Aboelez, M. S. A. Shaykhon, S. A. Ahmed, G. E.-D. A. Abuo-Rahma and O. M. Elhady, New nicotinic acid-based 3, 5-diphenylpyrazoles: Design, synthesis and antihyperlipidemic activity with potential NPC1L1 inhibitory activity, *Mol. Diversity*, 2021, **25**, 673–686.
15 T. Yang, W. Zhang and S. Cao, Discovery of highly potent and selective EGFR(T790M/L858R) TKIs against NSCLC based on molecular dynamic simulation, *Eur. J. Med. Chem.*, 2022, **228**, 113984.
16 F. Sherbiny, A. Bayoumi and A. El-Morsy, Design, Synthesis, biological Evaluation, and molecular docking studies of novel Pyrazolo[3,4-d]Pyrimidine derivative scaffolds as potent EGFR inhibitors and cell apoptosis inducers, *Bioorg. Chem.*, 2021, **5**(116), 105325.
17 S. A. Ahmed, M. S. Kamel, M. O. Aboelez, X. Ma, A. A. Al-Karmalawy, S. A. Mousa, E. K. Shokr, H. Abdel-Ghany, A. Belal and M. A. El Hamd, Thieno [2, 3-b] thiophene derivatives as potential EGFRWT and EGFRT790M inhibitors with antioxidant activities: Microwave-assisted synthesis and quantitative in vitro and in silico studies, *ACS Omega*, 2022, **7**, 45535–45544.
18 T. Yadav, S. G. Moin and M. A. Kumar, Review on Fused Pyrimidine Systems as EGFR Inhibitors and Their Structure-Activity Relationship, *Front. Chem.*, 2022, **2**(10), 861288.
19 M. M. Elsayed, M. O. Aboelez, B. E. Elsadek, H. A. Sarhan, K. A. Khaled, A. Belal, A. Khames, Y. A. Hassan, A. A. Abdel-Rheem and E. B. Elkaeed, Tolmetin sodium fast dissolving tablets for rheumatoid arthritis treatment: preparation and optimization using Box-Behnken design and response surface methodology, *Pharmaceutics*, 2022, **14**, 880.
20 N. Jain, J. Xu, R. M. Kanojia, F. Du, G. Jian-Zhong, E. Pacia, M.-T. Lai, A. Musto, G. Allan, G. Reuman and M. Cousineau, Identification and Structure– Activity Relationships of Chromene-Derived Selective Estrogen Receptor Modulators for Treatment of Postmenopausal Symptoms, *J. Med. Chem.*, 2009, **52**, 7544–7569.
21 A.-E.-B. A Ghattas, A. Khodairy, H. M. Moustafa, B. R. Hussein, M. M. Farghaly and M. O. Aboelez, Synthesis, in vitro antibacterial and in vivo anti-inflammatory activity of some new pyridines, *Pharm. Chem. J.*, 2017, **51**, 652–660.
22 A. H. Moustafa, W. W. Ahmed, M. F. Awad, M. O. Aboelez, A. Khodairy and A. A. Amer, Eco-friendly and regiospecific intramolecular cyclization reactions of cyano and carbonyl groups in N, N-disubstituted cyanamide, *Mol. Diversity*, 2022, **26**(5), 2813–2823.
23 L. Kujtan and J. Subramanian, Epidermal growth factor receptor tyrosine kinase inhibitors for the treatment of non-small cell lung cancer, *Expert Rev. Anticancer Ther.*, 2019, **19**(7), 547–559.
24 H. Ezelarab, H. Hassan, S. Abbas, T. Ali and E. Beshr, The main biotargets of indole or 2-oxoindole-based hybrids acting as promising antiproliferative agents, *J. Adv. Biomedical Pharm. Sci.*, 2023, **6**, 174–183, DOI: **10.21608/jabps.2023.217559.1190**.
25 H. A. A. Ezelarab, *et al.*, New antiproliferative 3-substituted oxindoles inhibiting EGFR/VEGFR-2 and tubulin polymerization, *Mol. Diversity*, 2024, **28**, 563–580.
26 M. O. Aboelez, M. S. Kamel, A. Belal, A. E. Abdel-Aziz, H. Abourehab, A. M. Abdel-Ghany, E. Hamd and M. A. E. A. El-Remaily, Microwave-assisted synthesis, spectroscopic characterization, and biological evaluation of fused thieno [2, 3-d] pyrimidines as potential anti-cancer agents targeting EGFRWT and EGFRT790M, *Mol. Diversity*, 2022, **27**(2), DOI: **10.1007/s11030-022-10477-7**.
27 R. Rosell, E. Carcereny, *et al.*, **Erlotinib** versus standard chemotherapy as first-line treatment for European patients with advanced EGFR mutation-positive non-small-cell lung cancer (EURTAC): a multicentre, open-label, randomised phase 3 trial, *Lancet Oncol.*, 2012, **13**(3), 239–246.
28 V. Di Noia, A. D'Aveni, E. D'Argento, S. Rossi, P. Ghirardelli, P. L. Bortolotti, V. Vavassori, E. Bria and G. Ceresoli, Treating disease progression with **osimertinib** in EGFR-mutated non-small-cell lung cancer: novel targeted agents and combination strategies, *ESMO Open*, 2021, **6**(6), 100280.
29 G. Xu, M. C. Abad, *et al.*, 4-Amino-6-arylamino-pyrimidine-5-carbaldehyde hydrazones as potent ErbB-2/EGFR dual kinase inhibitors, *Bioorg. Med. Chem. Lett.*, 2008, **18**, 4615–4619.
30 M. S. Kamel, M. O. Aboelez, M. R. Elnagar, E. K. Shokr, H. M. R. M. Selim, H. E. Selim, H. E. Abdel-Ghany, A. M. A. Drar, M. A. BelalEl Hamd and A. A. Abd El Aleem, Green Synthesis Design, Spectroscopic Characterizations, and Biological Activities of Novel Pyrrole Derivatives: An Application to Evaluate Their Toxic Effect on Cotton Aphids, *ChemistrySelect*, 2022, **7**(40), e202203191.
31 S. Sigismund, D. Avanzato and L. Lanzetti, Emerging functions of the EGFR in cancer, *Mol. Oncol.*, 2018, **12**(1), 3–20.
32 H. A. A. Ezelarab, S. H. Abbas, M. A. S. Abourehab, M. Badr, S. Sureram, P. Hongmanee, P. Kittakoop, G. E.-D. A. Abuo-Rahma and H. A. Hassan, Novel antimicrobial ciprofloxacin-pyridinium quaternary ammonium salts with improved physicochemical properties and DNA gyrase inhibitory activity, *Med. Chem. Res.*, 2021, **30**, 2168–2183, DOI: **10.1007/s00044-021-02798-3**.
33 F. Francesca, T. Annachiara, C. Valentina, P. Luca, M. Luca, P. Daniele and R. Giulio, Structure-activity exploration of a small-molecule allosteric inhibitor of T790M/L858R double mutant EGFR, *J. Enzyme Inhib. Med. Chem.*, 2023, **38**(1), 239–245.
34 E. Abdelkreem, S. M. Mahmoud, M. O. Aboelez and M. Abd El Aal, Nebulized magnesium sulfate for treatment of

persistent pulmonary hypertension of newborn: a pilot randomized controlled trial, *Indian J. Pediatr.*, 2021, **88**, 771–777.

35 K. K. Ang, B. A. Berkey, X. Tu, *et al.*, Impact of epidermal growth factor receptor expression on survival and pattern of relapse in patients with advanced head and neck carcinoma, *Cancer Res.*, 2002, **62**(24), 7350–7356.

36 P. Matada, N. Abbas, S. Dhiwar, *et al.*, Design, Synthesis, In Silico and In Vitro Evaluation of Novel Pyrimidine Derivatives as EGFR Inhibitors, *Anti-Cancer Agents Med. Chem.*, 2021, **21**(4), 451–461.

37 H. A. El-Sayeda, A. H Moustafaa, A. A. Faddab and K. E. Abd El-Rahmana, Pyrazole and Nicotinonitrile Derivatives Synthesized from Sulfa Drugs, and Their Antibacterial Activity, *Russ. J. Gen. Chem.*, 2019, **89**(2), 339–347.

38 K. Terufumi, C. Ignacio, C. Manuel, *et al.*, Targeted treatment for unresectable EGFR mutation-positive stage III non-small cell lung cancer: Emerging evidence and future perspectives, *Lung Cancer*, 2024, **187**, 107414, DOI: **10.1016/j.lungcan.2023.107414**.

39 W. Yahua, D. Bin., L. Chengliu, J. Xiaohui and L. Jinhuo, LAPS score for individualized treatment of advanced EGFR-mutated non-small cell lung cancer receiving EGFR-TKIs with or without bevacizumab, *Ann. Med.*, 2023, **55**(2), 2257227, DOI: **10.1080/07853890.2023.2257227**.

40 C. H. Dai, Y. Shu, *et al.*, YM155 sensitizes non-small cell lung cancer cells to EGFR-tyrosine kinase inhibitors through the mechanism of autophagy induction, *Biochim. Biophys. Acta, Mol. Basis Dis.*, 2018, **1864**(12), 3786–3798.

41 A. Kassab, Pyrazolo[3,4-d]pyrimidine scaffold: A review on synthetic approaches and EGFR and VEGFR inhibitory activities, *Arch. Pharm.*, 2023, **356**(1), 2200424.

42 A. Gazdar, Activating and resistance mutations of EGFR in non-small-cell lung cancer: role in clinical response to EGFR tyrosine kinase inhibitors, *Oncogene*, 2009, **28**(1), S24–S31.

43 Y. Guo, L. Yang, L. Liu, *et al.*, Comparative study of clinicopathological characteristics and prognosis between combined and pure small cell lung cancer (SCLC) after surgical resection, *Thorac. Cancer*, 2020, **11**(10), 2782–2792.

44 X. Wang, Y. Guo, L. Liu, *et al.*, YAP1 protein expression has variant prognostic significance in small cell lung cancer (SCLC) stratified by histological subtypes, *Lung Cancer*, 2021, **2**(160), 166–174.

45 A. Belal, M. A. Elanany, E. Y Santali, A. A. Al-Karmalawy, M. O. Aboelez, A. H. Amin, M. H. Abdellattif, A. B. Mehany and H. Elkady, Screening a Panel of Topical Ophthalmic Medications against MMP-2 and MMP-9 to Investigate Their Potential in Keratoconus Management, *Molecules*, 2022, **27**, 3584.

46 W. Pao, V. A. Miller, K. A. Politi, *et al.*, Acquired resistance of lung adenocarcinomas to **gefitinib** or **erlotinib** is associated with a second mutation in the EGFR kinase domain, *PLoS Med.*, 2005, **2**(3), 73–92.

47 H. A. A. Ezelarab, T. F. S. Ali, S. H. Abbas, H. A. Hassan and E. A. M. Beshr, Indole-based FLT3 inhibitors and related scaffolds as potential therapeutic agents for acute myeloid leukemia, *BMC Chem.*, 2023, **17**, 73.

48 M. M. A. Elsayed, M. O. Aboelez, M. S. Mohamed, R. A. Mahmoud, A. A. El-Shenawy, *et al.*, Tailoring of Rosuvastatin Calcium and Atenolol Bilayer Tablets for the Management of Hyperlipidemia Associated with Hypertension: A Preclinical Study, *Pharmaceutics*, 2022, **14**(8), 1629.

49 B. Kaghazchi, L. Um and M. Elshani, Spatial Analysis of NQO1 in Non-Small Cell Lung Cancer Shows Its Expression Is Independent of NRF1 and NRF2 in the Tumor Microenvironment, *Biomolecules*, 2022, **12**(11), 122–135.

50 D. Todsaporn, A. Zubenko, V. Kartsev, T. Aiebchun, P. Mahalapbutr, A. Petrou, A. Geronikaki, L. Divaeva, V. Chekrisheva, L. Yildiz, K. Choowongkomon and T. Rungrotmongkol, Discovery of Novel EGFR Inhibitor Targeting Wild-Type and Mutant Forms of EGFR: In Silico and In Vitro Study, *Molecules*, 2023, **28**(7), 3014.

51 S. Sogabe, Y. Kawakita, S. Igaki, H. Iwata, H. Miki, D. R. Cary, T. Takagi, S. Takagi, Y. Ohta and T. Ishikawa, Structure-Based Approach for the Discovery of Pyrrolo[3,2- d] Pyrimidine-Based EGFR T790M/L858R Mutant Inhibitors, *ACS Med. Chem. Lett.*, 2013, **4**(2), 201–205.

52 M. S. Abdelbaset, M. Abdel-Aziz and M. Ramadan, Discovery of novel thienoquinoline-2-carboxamide chalcone derivatives as antiproliferative EGFR tyrosine kinase inhibitors, *Bioorg. Med. Chem.*, 2019, **27**, 1076–1086.

53 F. Doganc, I. Celik, G. Eren, M. Kaiser, R. Brun and H. Goker, Synthesis, in vitro antiprotozoal activity, molecular docking and molecular dynamics studies of some new monocationic guanidinobenzimidazoles, *Eur. J. Med. Chem.*, 2021, **221**, 113545.

54 A. Daina, O. Michielin and V. Zoete, SwissADME: A free web tool to evaluate pharmacokinetics, drug-likeness and medicinal chemistry friendliness of small molecules, *Sci. Rep.*, 2017, **7**, 1–13.

55 A. Mavani, A. Ovung, A. Luikham, *et al.*, Biophysical and molecular modeling evidences for the binding of sulfa molecules with hemoglobin, *J. Biomol. Struct. Dyn.*, 2023, **41**(9), 3779–3790.

56 K. AL Azzam, SwissADME and pkCSM Webservers Predictors: an integrated Online Platform for Accurate and Comprehensive Predictions for In Silico ADME/T Properties of Artemisinin and its Derivatives, *Compl. Use of Min. Resour.*, 2022, **325**(2), 14–21.

57 A. Daina and V. Zoete, A BOILED-Egg To Predict Gastrointestinal Absorption and Brain Penetration of Small Molecules, *ChemMedChem*, 2016, **11**, 1117–1121.

58 C. A. Lipinski, F. B. Lombardo, W. Dominy and P. J. Feeney, Experimental and computational approaches to estimate solubility and permeability in drug discovery and development settings, *Adv. Drug Delivery Rev.*, 2012, **64**, 4–17.

59 L. Yuanyuan, K. Wang, M. Jiaxuan, W. Zhengcong, Z. Qiujin and J. Yongguo, Effect of yolk spheres as a key histological structure on the morphology, character, and oral sensation of boiled egg yolk gel, *Food Chem.*, 2023, **424**, 136380.

60 H. A. A. Ezelarab, H. A. Hassan, G. E.-D. A. Abuo-Rahma and S. H. Abbas, Design, synthesis, and biological investigation of quinoline/ciprofloxacin hybrids as antimicrobial and anti-proliferative agents, *J. Iran. Chem. Soc.*, 2023, **20**, 683–700.

61 M. O. Aboelez, H. A. A. Ezelarab, G. Alotaibi, *et al.*, Inflammatory setting, therapeutic strategies targeting some pro-inflammatory cytokines and pathways in mitigating ischemia/reperfusion-induced hepatic injury: a comprehensive review, *Naunyn-Schmiedeberg's Arch. Pharmacol.*, 2024, **1**, 17.

62 M. A. E. El-Remaily, M. O. Aboelez and H. A. A. Ezelarab, Guanidine dicycloamine-based analogs: green chemistry synthesis, biological investigation, and molecular docking studies as promising antibacterial and antiglycation leads, *Mol. Diversity*, 2024, **1**, 23.